hydrology

MDPI

Article

An Integrated Approach to the Regional Estimation of Soil Moisture

Luis Pastor Sánchez-Fernández [1,*], Diego Alberto Flores-Carrillo [1] and Luis Alejandro Sánchez-Pérez [2]

[1] Centro de Investigación en Computación, Instituto Politécnico Nacional, Mexico City CP 07738, Mexico
[2] Department of Electrical and Computer Engineering, University of Michigan, Dearborn, MI 48128, USA
* Correspondence: lsanchez@cic.ipn.mx

Abstract: Automatic or smart irrigation systems benefit irrigation water management. However, measurement sensor networks in automatic irrigation systems are complex, and maintenance is essential. Regional soil moisture estimation avoids the multiple measurements necessary when deploying an irrigation system. In this sense, a fuzzy estimation approach based on decision-making (FEADM) has been used to obtain soil moisture *point* estimates. However, FEADM requires intelligent weather adjustment based on spatial features (IWeCASF) to perform *regional* soil moisture estimation. The IWeCASF-FEADM integrated approach for *regional* soil moisture estimation is developed in this work. IWeCASF provides the inputs for FEADM. FEADM is performed R times; R is the number of checkpoints at which a *point* estimate is obtained. In this way, *regional* estimation is achieved when the set of R soil moisture *point* estimates is completed. Additionally, IWeCASF-FEADM considers the irrigation water records, which are not included in either method individually. This method can detect when the soil moisture is deficient in a region, allowing actions to prevent water stress. This *regional* estimation reduces an irrigation system's operational and maintenance complexity. This integrated approach has been tested over several years by comparing the results of *regional* soil moisture estimation with measurements obtained at many points in the study region.

Keywords: soil moisture regional estimate; point estimation; weather condition adjustment; region spatial features

Citation: Sánchez-Fernández, L.P.; Flores-Carrillo, D.A.; Sánchez-Pérez, L.A. An Integrated Approach to the Regional Estimation of Soil Moisture. *Hydrology* **2024**, *11*, 170. https://doi.org/10.3390/hydrology11100170

Academic Editors: Beatrice Monteleone, Hailong Yin and Iolanda Borzì

Received: 19 September 2024
Revised: 8 October 2024
Accepted: 9 October 2024
Published: 11 October 2024

1. Introduction

Currently, enhancing irrigation water consumption is vital in appropriately exploiting agricultural resources. As a result, improved automatic irrigation systems [1–4], or intelligent systems for water management, have been developed [5–8].

A set of checkpoints is commonly deployed throughout an irrigation region when an automatic irrigation system is used [9,10]. At each checkpoint, soil moisture measurements determine the irrigation water requirements. Therefore, a measurement sensor network is needed [11]. The soil moisture determined within the irrigation region based on measurements can provide a very accurate representation; nevertheless, the inherent complexity of its implementation and maintenance is prominent [12,13].

An intelligent model for the estimation of soil moisture can reduce the complexity involved in measuring soil moisture and, consequently, the costs of automatic irrigation systems. Hydrological models can estimate soil moisture based on land surface models and the weather conditions [14–16]. These models can accurately estimate soil moisture; however, their development complexity is high due to the difficulties in acquiring the input data and the assumptions performed during model development. Moreover, soil moisture can be obtained with soil water balance calculations, which are easy to implement while being very accurate, because these calculations require regular recalibration [17–19].

Soil moisture remote sensing can be performed at any time without being affected by cloud cover, vegetation or night conditions; it is achieved using satellite microwave

sensors [20,21]. Nevertheless, the scale (~25 to 50 km) and the complexity in implementing these microwave sensors render soil moisture remote sensing an alternative that is only suitable for huge farmland systems. Earth observation technologies are essential in monitoring sustainable application development at different scales; these include soil moisture estimations [22], soil moisture mapping services [23], and soil moisture estimation, combining satellite radar measurements and land surface modeling [24], among others.

Artificial neural networks (ANNs) [25–27] and support vector machines (SVMs) [28,29] are used for soil moisture estimation, and they have different advantages. These models enable accurate estimation but present restrictions for implementation in small farms. An SVM performs better than an ANN when an ensemble Kalman filter (EnKF) is utilized [30,31]. However, both approaches require many tests to obtain an accurate soil moisture estimate [32,33].

Fuzzy logic is a powerful technique for analyzing hydrologic elements and decision making in water resources. Many issues connected to hydrology frequently deal with imprecision and vagueness, and they can be very well handled by fuzzy logic-based models [34]. Other works are related to optimizing irrigation systems; the authors propose using several water microturbines to generate sustainable energy without affecting crop irrigation efficiency [35]. In this sense, sustainable and energy-efficient agricultural practices require integrating different systems that utilize water adequately, including small irrigation regions or greenhouses [36].

A model was developed to estimate the soil *point* moisture based on decision-making using a fuzzy inference system (FEADM) [32]. FEADM obtains *point* estimates of the soil moisture from the measurements of certain variables, such as the air temperature, rain, solar radiation, wind speed, and evapotranspiration, using a wireless environmental monitoring station that uses radio frequency signals to transmit data (details in [32]).

FEADM models the relationships among the soil moisture, weather conditions, and checkpoint features where the estimation is performed. FEADM is suitable for *regional* soil moisture estimation when obtaining *point* soil moisture estimates at several regional checkpoints. Nevertheless, FEADM requires the weather conditions at every checkpoint, but measuring the weather conditions at several checkpoints within a region is impractical.

The weather conditions remain similar within a specific region [37,38], although its landscape features can lead to inconsistencies. Many analyses and experiments support the significance of such discrepancies in the regional weather conditions. In this sense, an intelligent weather condition adjustment based on spatial features (IWeCASF) [39] was developed. This model permits the weather conditions to be obtained anywhere within a region, since IWeCASF considers the weather condition inconsistencies mentioned above. IWeCASF requires the measured weather conditions at a single checkpoint, and, from these measurements, IWeCASF determines the weather conditions at any other checkpoint by performing intelligent adjustment. This intelligent adjustment considers the relationships between the weather conditions and the checkpoints' spatial features.

Moreover, both methods consider the weather conditions and soil and crop features to be essential to determine the soil moisture content.

Nevertheless, as with conventional irrigation systems, the integrated approach aims to determine the soil moisture content at several checkpoints scattered across an irrigation region. Thus, it eliminates the need for the full implementation of the conventional irrigation system and mitigates its maintenance complexity [12,13] by estimating the *regional* soil moisture instead of measuring it.

Measuring the weather conditions at several checkpoints located in a region can be more complex than measuring the soil moisture as in conventional irrigation systems. For example, in a region, as depicted in Figure 1, measuring the weather conditions at each $R = 12$ checkpoints, $P^{r=1,2,\ldots,R}$, is more complex than simply measuring the soil moisture at each checkpoint, P^r, due to the requirements of the measuring devices. However, the weather conditions remain similar within a region [37,38]. For example, given an irrigation region, as shown in Figure 1, the air temperature can be highly similar at checkpoints P^0,

P^4, and P^8. The same can be true for other weather conditions, such as solar radiation, which can even be similar at checkpoints P^0, P^4, P^8, and P^{11}, which are located relatively far apart.

Figure 1. Example of application of integrated soil moisture estimation approach for 12 checkpoints. In the image, * FEADM [32]; ** IWeCASF [39]; and *** addition of irrigation water record δ_{x_r,y_r} of checkpoint P^r.

Thus, the weather conditions anywhere within a specific region can be determined by measuring only one checkpoint (the primary checkpoint). Moreover, despite the similarity of the weather conditions, there can be minor variations due to the spatial features of the region. For example, in the region in Figure 1, the air temperature is almost the same at most of the checkpoints, as described in the previous example; however, there could be a noticeable air temperature difference between checkpoint P^4, which is a grassland area, and the checkpoints P^2 or P^{10}, which are mainly tree-covered areas. The tree-covered areas at checkpoints P^2 or P^{10} partially block solar radiation at the soil level, which can result in a cooler air temperature. Therefore, considering that the spatial features influence the weather conditions, these variations within a specific region can be determined if a spatial analysis is performed. This is the aim of the "intelligent weather condition adjustment based on spatial features" (IWeCASF) model [39].

In brief, the IWeCASF-FEADM integrated approach utilizes IWeCASF to determine the weather conditions at any checkpoint where a *point* soil moisture estimation is performed with FEADM. Figure 1 demonstrates an application of the integrated approach for *regional* soil moisture estimation. Firstly, the weather conditions $C^0_{i=1,2,...,I}$ are measured at the primary checkpoint (P^0), and then the measured weather conditions $C^0_{i=1,2,...,I}$ and the rest of the inputs required by IWeCASF are processed to determine the adjusted weather conditions $C^r_{i=1,2,...,I}$ at each checkpoint P^r. The adjusted weather conditions $C^r_{i=1,2,...,I}$ for checkpoint P^r and the irrigation water record are introduced to FEADM to perform the *point* soil moisture estimation. In this way, the set of *point* soil moisture estimates at each checkpoint $P^{r=1,2,...,R}$ is defined as the *regional* soil moisture estimation.

The locations of checkpoints $P^{r=1,2,...,R}$ are determined by the number of zones identified in conventional irrigation systems, but, if a more detailed *regional* soil moisture estimate is required, more checkpoints must be defined. This approach is suitable for use in different regions; it is only necessary to modify the input parameters.

The theoretical framework presents mathematical formulations and symbols supporting the analyses. However, they do not limit other readers since the work includes many descriptions, detailed figures, diagrams, and tables.

This work hypothesizes that linking FEADM with ICASF allows *regional* soil moisture estimation (in a specific region). Likewise, the IWeCASF-FEADM approach for *regional* soil moisture estimation can reduce the implementation and maintenance complexity of conventional automatic irrigation systems and their inherent costs.

In this study, the integrated approach to *regional* soil moisture estimation (called the integrated approach) is developed. This approach utilizes the joint IWeCASF-FEADM to perform a *regional* analysis (set of *point* estimates) of soil moisture; additionally, the irrigation water supply is introduced to FEADM to complement the rainfall for the processing of a broader set of water supply records.

Based on mathematical formulations, the integrated approach determines a *regional* estimation of the soil moisture anywhere within a region through image geoprocessing algorithms and fuzzy inference systems. The intelligent weather condition adjustment through spatial features (IWeCASF) [39] and the soil moisture fuzzy *point* estimation model based on decision-making (FEADM) [32] exploit the advantages of evaluating soil moisture with FEADM but eliminate its limitations.

2. Materials and Methods

Figure 2 depicts an overview of the integrated IWeCASF-FEADM approach for the *regional* estimation of soil moisture. The integrated method developed herein accomplishes *regional* soil moisture estimation (Re) from a set of soil moisture *point* estimates ($Sm^{r=1,2,\ldots,R}$). The integrated approach requires as inputs the satellite imagery of the estimation region, as well as the data of the soil and crop zones ($M^{t=1,2,\ldots,T}$) identified within this region. Moreover, the locations of the checkpoints ($P^{r=0,1,2,\ldots,R}$), the weather conditions measured ($C^{0}_{i=1,2,\ldots,I}$) at one of the checkpoints (primary checkpoint P^0) and the water irrigation record ($\Delta^{r=1,2,\ldots,R}$) are needed. The integrated approach links the IWeCASF model [39] and the fuzzy estimation approach based on decision-making (FEADM) [32]. IWeCASF determines the weather conditions ($C^{r}_{i=1,2,\ldots,I}$) at every checkpoint (P^r), which are utilized by FEADM to obtain each soil moisture point estimate (Sm^r). The set of soil moisture point estimates ($Re = \{Sm^1, Sm^2, \ldots, Sm^R\}$) of all checkpoints ($P^r$) represents the *regional* estimation of soil moisture (Re).

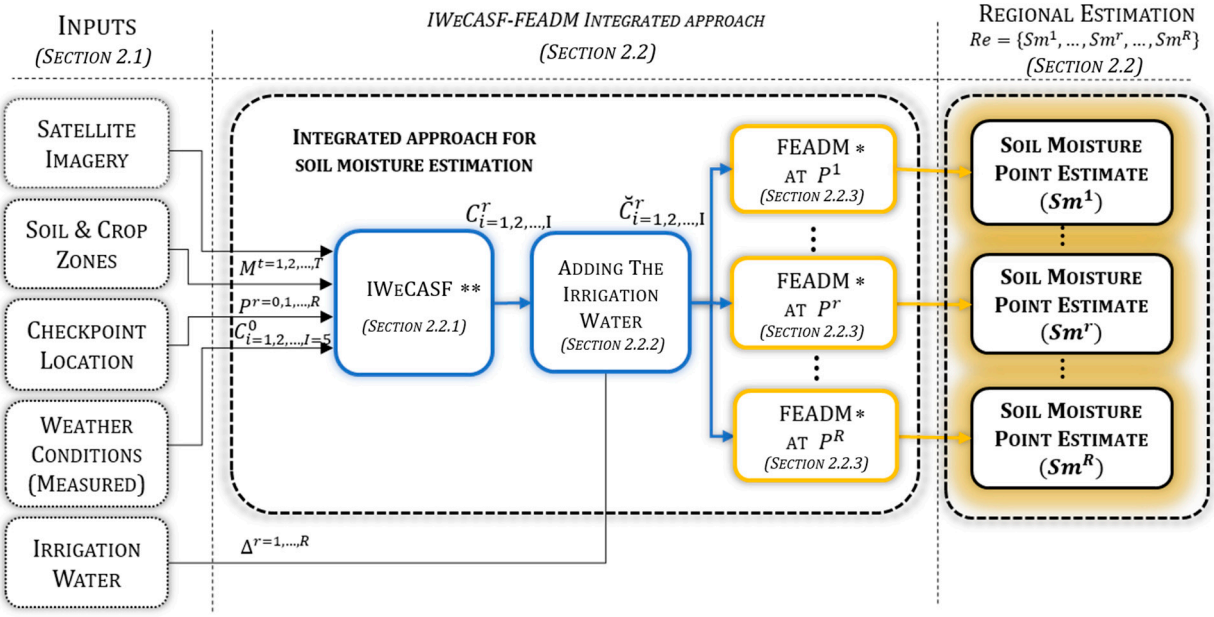

** Sánchez-Fernández, L.P. et al., 2024. Computer Model for an Intelligent Adjustment of Weather Conditions Based on Spatial Features for Soil Moisture Estimation. Mathematics 2024, 12, 152.

* Flores-Carrillo, D.A. et al., 2017. Soil moisture Fuzzy Estimation Approach based on Decision-Making. Environmental Modelling & Software 2017, 91, 223.

Figure 2. Overview of integrated approach for *regional* estimation of soil moisture. In the image, ** IWeCASF [39] and * FEADM [32].

2.1. Inputs

The integrated approach conforms with the IWeCASF-FEADM linkage; therefore, certain inputs are required by these two models. As defined in [39], the information necessary to develop IWeCASF includes the satellite imagery, soil and crop zones, checkpoint locations, and measured weather conditions; meanwhile, FEADM [32] only needs the weather conditions as inputs.

The satellite imagery corresponds to images (with a scale of 1:10,000) obtained with the USGS National Map Viewer from Landsat in March 2017. QGIS [40] is used for processing. The images are divided into S sectors, resulting in pairwise sectors $s(x, y)$, where $x = 1, 2, \ldots, X$, $y = 1, 2, \ldots, Y$, X is the image width, and Y is the image height.

The soil and crop zones constitute a geographic data set organized in two databases. The first has the region's geo-information divided into zones concerning the soil texture, field capacity and available water content [39,41,42]. The second database includes the region's geo-information divided into zones according to the crop type and its development stage [39,43]. Both databases are utilized to define the feature matrices $M^{t=1,2,\ldots,T}$, where T is the total number of features identified; in this case, $T = 3$ ($M^{t=1}$ soil type, $M^{t=2}$ crop type, and $M^{t=3}$ development stage). The size of the feature matrices is XxY, defined by the S sectors established in the satellite imagery. Additionally, elements $m^{t}_{x,y}$ of feature matrices M^{t} contain the number of pixels at sector $s(x, y)$ that belong to a feature [39].

Moreover, the checkpoint location $s(x_r, y_r)$ is another input; it denotes the sector $s(x, y)$ where checkpoint P^r is located, and it is used to identify the particular features at this location. Additionally, the input weather conditions $C^{0}_{i=1,2,\ldots,I}$ are measured at the primary checkpoint P^0 with an integrated sensor suite [32], as defined in Table 1.

Table 1. Weather conditions $C^{r}_{i=1,2,\ldots,I}$, $(I = 5)$ measured at primary checkpoint $r = 0$.

$C^{0}_{i=1,2,\ldots,I}$	Variable
C^{0}_{1}	Temperature (T)
C^{0}_{2}	Rain (R)
C^{0}_{3}	Solar radiation (Sr)
C^{0}_{4}	Wind speed (Ws)
C^{0}_{5}	Evapotranspiration (Et)

The input irrigation water is a matrix $\Delta = \left(\delta_{x_r,y_r}\right)_{X*Y}$ obtained from a geographic database; it denotes the amount of irrigation water supplied in each sector $s(x, y)$ from the irrigation region. This input, as a complement to the rain data C^{r}_{2}, is used in the integrated approach to determine the actual water supply in a sector $s(x_r, y_r)$. The external subscripts X and Y are as follows: X is the image width and Y is the image height.

2.2. IWeCASF-FEADM Integrated Approach

The IWeCASF-FEADM integrated approach is composed of two stages. The first stage is IWeCASF [39]. Firstly, IWeCASF's results are combined with the irrigation water record; afterwards, they are supplied as input to the second stage. The second stage is FEADM [32], which determines the soil moisture *point* estimates at each checkpoint. The linkage of IWeCASF and FEADM gives a *regional* soil moisture estimation as a *point* estimate set. Sections 2.2.1 and 2.2.2 present the details of the integration of IWeCASF and FEADM, respectively.

2.2.1. IWeCASF

IWeCASF [39] determines the weather conditions within a region, providing FEADM [32] with the inputs required for a *point* estimate. This goal is achieved by performing three tasks: landscape feature extraction, selecting specific landscape features at each checkpoint, and adjusting the weather conditions at each checkpoint. IWeCASF's inputs are the satellite imagery of the estimation region, the soil and crop zones, the checkpoint locations, and the

weather conditions measured at the primary checkpoint. As mentioned above, the results derived from IWeCASF (the weather conditions at each checkpoint) are utilized as inputs by FEADM. The five stages (A to F) are described as follows:

A. Landscape feature extraction: This is the stage of IWeCASF in which an image is processed to define the landscape feature matrices $F^{l=1,2,\ldots,L}$ of the irrigation region's satellite imagery. The landscape feature matrices $F^{l=1,2,\ldots,L}$ are necessary to obtain a steady adjustment factor. L is the total number of landscape features; in this case, $L = 5$ (grassland, tree cover area, buildings, elevation, and spatial configuration). First, the image is enhanced through color space conversion from red, green, and blue (RGB) to the International Commission of Lighting Luminosity band A/band B color space (CIELAB) [44]. Afterwards, a decorrelation process is implemented to simplify the image color segmentation. Then, the landscape feature matrices F^l are defined, where each matrix represents a landscape feature identified from the image. Color segmentation assigns each pixel of the image to one prototype cluster $K_{l=1,2,\ldots,L}$, which represents a landscape feature, using the objective function G defined in Equation (1), as described in [44].

$$G = \sum_{l=1}^{L} \sum_{\vec{a}_d \in K_l} \left\| \vec{a}_d - \vec{b}_l \right\|^2 \quad (1)$$

When color segmentation is completed, the image is separated pixel by pixel into $L = 5$ landscape features, which consist of the grassland (l =1), tree cover area (l = 2), buildings (l = 3), elevation (l = 4), and spatial configuration (l =5). However, to define the landscape feature matrices, the image is divided into sectors $s(x, y)$, where $x = 1, 2, \ldots, X$ and $y = 1, 2, \ldots, Y$. X is the width and Y is the height of the satellite image divided into S sectors. Thus, each element $f^l_{x,y}$ = (number of pixels) of a landscape feature matrix $F^l = \left(f^l_{x,y}\right)_{X*Y}$ denotes the number of pixels at sector $s(x, y)$ corresponding to the landscape feature l.

B. Checkpoint landscape feature selection: In this stage, the input locations $s(x_r, y_r)$ of checkpoints $P^{r=1,2,\ldots,R}$ and the feature matrices $M^{t=1,2,\ldots,T} = \left(m^t_{x,y}\right)_{XxY}$ are utilized. Additionally, the landscape feature matrices $F^{l=1,2,\ldots,L} = \left(f^l_{x,y}\right)_{X*Y}$ extracted from the image are required. The checkpoint location $s(x_r, y_r)$ selects from its respective matrices the elements $f^l_{x=x_r,\, y=y_r}$ and $m^t_{x=x_r,\, y=y_r}$ that represent the landscape feature l or the feature t at sector $s(x = x_r,\ y = y_r)$. As a result of this selection, the particular feature vector $\phi^r\left(F^l, M^t, P^r\right)$ is obtained, as shown in Equation (2). The elements of this vector $\phi^r\left(F^l, M^t, P^r\right)$ are defined as the number of pixels at sector $s(x = x_r, y = y_r)$. Then, the elements of the particular feature vector $\phi^r\left(F^l, M^t, P^r\right)$ are represented as a percentage of the particular feature vector $\phi^r\left(F^l, M^t, P^r\right)$, as described in Equation (3).

$$\phi^r\left(F^l, M^t, P^r\right) = \left[f^1_{x_r,y_r}, f^2_{x_r,y_r}, \ldots, f^L_{x_r,y_r}, m^1_{x_r,y_r}, m^2_{x_r,y_r}, \ldots, m^T_{x_r,y_r}\right] \quad (2)$$

$$\phi^r\left(F^l, M^t, P^r\right) = \left[\phi^r_{e=1}, \phi^r_{e=2}, \ldots, \phi^r_{e=L}, \phi^r_{e=L+1}, \phi^r_{e=L+2}, \ldots, \phi^r_{e=E}\right] \quad (3)$$

C. Fuzzy adjustment: This is performed to determine the weather conditions $C^0_{i=1,2,\ldots,I}$ at checkpoint P^r after the particular feature vector $\mathbf{\Phi}^r\left(F^l, M^t, P^r\right)$ is identified. Fuzzy adjustment begins with the fuzzification of the weather conditions measured, $C^0_{i=1,2,\ldots,I}$, and of the landscape feature vector $\mathbf{\Phi}^r\left(F^l, M^t, P^r\right)$. A sigma function, an L-shaped function, and a triangle function are used for fuzzifying, as defined in [39]. The fuzzy weather

conditions $\widetilde{C}_i^0(v_i)$, where v_i is the current value of weather condition C_i^0, are of the form defined in Equations (4)–(8).

$$\widetilde{C}_1^0(v_i) = \left\{\tilde{c}_{1,1}^0, \tilde{c}_{1,2}^0, \cdots, \tilde{c}_{1,5}^0\right\} \quad | \text{ Temperature} \tag{4}$$

$$\widetilde{C}_2^0(v_i) = \left\{\tilde{c}_{2,1}^0, \tilde{c}_{2,2}^0, \cdots, \tilde{c}_{2,5}^0\right\} \quad | \text{ Rain} \tag{5}$$

$$\widetilde{C}_3^0(v_i) = \left\{\tilde{c}_{3,1}^0, \tilde{c}_{3,2}^0 \cdots, \tilde{c}_{3,5}^0\right\} \quad | \text{ Solar radiation} \tag{6}$$

$$\widetilde{C}_4^0(v_i) = \left\{\tilde{c}_{4,1}^0, \tilde{c}_{4,2}^0, \cdots, \tilde{c}_{4,5}^0\right\} \quad | \text{ Wind speed} \tag{7}$$

$$\widetilde{C}_5^0(v_i) = \left\{\tilde{c}_{5,1}^0, \tilde{c}_{5,2}^0, \cdots, \tilde{c}_{5,5}^0\right\} \quad | \text{ Evapotranspiration} \tag{8}$$

Moreover, to fuzzify the landscape feature vectors $\phi^r\left(F^l, M^t, P^r\right)$, it is necessary to compare the landscape features $\phi^r\left(F^l, M^t, P^r\right)$ at the checkpoint where the adjustment is performed and the landscape features at the primary checkpoint $\phi^0\left(F^l, M^t, P^0\right)$. This comparison $\phi^{0,r}$ is executed using Equation (9).

$$\phi^{0,r} = \phi^0\left(F^l, M^t, P^0\right) - \phi^r\left(F^l, M^t, P^r\right) = \left[\phi_{e=1}^0 - \phi_{e=1}^r, \phi_{e=2}^0 - \phi_{e=2}^r, \cdots, \phi_{e=E}^0 - \phi_{e=E}^r\right] \tag{9}$$

Then, the elements of comparison $\phi^{0,r}$ are fuzzified using membership functions, i.e., the form triangle, L-shaped or sigma-shaped function, as described in [39]. In this way, the fuzzy particular feature matrix $\widetilde{\phi}^r$ is obtained, as shown in Equation (10).

$$\widetilde{\phi}^r = \begin{bmatrix} \tilde{\phi}_{1,1}^r & \tilde{\phi}_{1,2}^r & \tilde{\phi}_{1,3}^r \\ \tilde{\phi}_{2,1}^r & \tilde{\phi}_{2,2}^r & \tilde{\phi}_{e,3}^r \\ \vdots & \vdots & \vdots \\ \tilde{\phi}_{E,1}^r & \tilde{\phi}_{E,1}^r & \tilde{\phi}_{E,3}^r \end{bmatrix} \tag{10}$$

D. Landscape adjustment: This stage models the influence of the particular checkpoint features $\phi^r\left(F^l, M^t, P^r\right)$ over the weather conditions measured $C_{i=1,2,\ldots,I}^0$. Landscape adjustment uses a fuzzy inference system (FIS), which receives as inputs the fuzzy particular feature matrix $\widetilde{\phi}^r$. This FIS utilizes a compound of $n = 1, 2, \ldots, N$ **IF THEN** rules, where $N = 245$ when modeling the adjustment factor according to the actual particular feature differences between the checkpoint P^r and the primary checkpoint P^0. The landscape adjustment FIS presents as output a steady adjustment factor element $\alpha_{r,i} | \; i = 1, 2, \ldots, I$, where I = 5 is the number of weather conditions. Each output is separated into $\lambda_{i,o} \mid o = 1, 2, \ldots, O$ output sets, with $O = 5$ according to [39]. The result of landscape adjustment is a weather condition steady adjustment factor $\alpha_{r,i}$ for each weather condition, which is gathered as $\Lambda_r = (\alpha_{r,i})_{1,I}$.

E. Variable adjustment: Before developing the variable adjustment, it is necessary to determine the certainty of the weather condition replication $\eta_{i=1,2,\ldots,I}$, which improves the modeling of inconsistent weather conditions such as rain (C_2^0). This certainty $\eta_{i=1,2,\ldots,I}$ is obtained using a distribution function, as in [39]. Afterwards, the certainty of the weather condition replication $\eta_{i=1,2,\ldots,I}$ and the weather conditions measured $C_{i=1,2,\ldots,I}^0$ are processed through the $Q = 445$ **IF THEN** rules of a second FIS (variable adjustment). Its result is associated with the output membership functions' variables $\beta_i \mid i = 1, 2, \ldots, I$ to model the influence of the weather conditions over the rest. As a result of defuzzification, a variable adjustment B factor is obtained.

F. Final adjustment: This gives the result of the weather conditions $C_{i=1,2,\ldots,I}^r$ at checkpoint P^r. Both the factors steady adjustment Λ_r and variable adjustment B are used to

determine the suggested adjustment of each weather condition C_i^r at checkpoint P^r. According to [39], the adjusted weather conditions C_i^r are obtained as shown in Equation (11).

$$C_i^r = (C_i^0)(1 + \alpha_{r,i} + \beta_i) \;\Big|\; r = 1, 2, \ldots, R; i = 1, 2, \ldots, I \tag{11}$$

2.2.2. Addition of Irrigation Water

IWeCASF's final result is the weather conditions $C^r_{i=1,2,\ldots,I}$ at any checkpoint within a region. In the first stage of the integrated IWeCASF-FEADM approach developed herein, these weather conditions $C^r_{i=1,2,\ldots,I}$, are used as the inputs of FEADM (second stage). A particular case is the weather condition $C^r_{i=2}$ (rain), which is complemented before being introduced to FEADM. Thus, the actual weather conditions $\check{C}_i^r$ supplied to FEADM are defined in Equation (12), in which the irrigation water record δ_{x_r,y_r} of checkpoint P^r is added to weather condition $C^r_{i=2}$ (rain) at checkpoint P^r. Meanwhile, the rest of the weather conditions remain the same.

$$\check{C}_i^r = \begin{cases} C_i^r + \delta_{x_r,y_r} & i = 2 \\ C_i^r & i \neq 2 \end{cases} \tag{12}$$

2.2.3. FEADM

The integrated IWeCASF-FEADM approach continues with the second FEADM stage [32]. FEADM is utilized to estimate the soil moisture content (point estimation of soil moisture Sm^r) in a delimited area (checkpoint P^r) as from the weather conditions determined with IWeCASF.

Furthermore, unlike conventional decision-making methods, FEADM not only selects the best decision alternative (qualitative result) but also estimates the actual value of an alternative when available (quantitative result). The aim is to select, from a set of soil moisture levels (defined in FEADM as alternatives $A_{k=1,2,\ldots,K}$), the best-assessed alternative according to the actual weather conditions $C_{i=1,2,\ldots,I}$ (defined in FEADM as decision criteria $C_{i=1,2,\ldots,I}$) and then estimate its actual value. Therefore, FEADM is executed at each checkpoint P^r, in which the actual weather conditions $\check{C}^r_{i=1,2,\ldots,I}$ derived from IWeCASF and modified with the addition of irrigation water are required as inputs. FEADM's result is a *point* soil moisture estimate Sm^r at checkpoint P^r. The three stages (A to C) are described as follows:

A. FEADM begins with a fuzzy analytical hierarchy process [32,45–47], which compares the relevance of each decision criterion (adjusted weather conditions derived from IWeCASF) over the rest. This comparison is performed for each decision criterion. The method developed by [45] and adapted by [46] is used in FEADM. As a result, a weight set $W = \{w_1, w_2, \ldots, w_I\}$ is obtained.

Firstly, a judgment matrix $\tilde{P}$ is defined as in Equation (13). The elements $\tilde{p}_{x,y}$ are triangle fuzzy numbers (TFN) that represent the relative importance values, which are derived from criteria pairwise comparison $\left(Ca_x, Ca_y\right)$, where $x = 1, 2, \ldots, I$ and $y = 1, 2, \ldots, I$.

$$\tilde{P} = \begin{array}{c} \\ C_1 \\ C_2 \\ \vdots \\ C_I \end{array} \begin{array}{c} \begin{array}{cccc} C_1 & C_2 & \cdots & C_I \end{array} \\ \begin{bmatrix} \tilde{p}_{1,1} & \tilde{p}_{1,2} & \cdots & \tilde{p}_{1,I} \\ \tilde{p}_{2,1} & \tilde{p}_{2,2} & \cdots & \tilde{p}_{2,I} \\ \vdots & \vdots & \ddots & \vdots \\ \tilde{p}_{I,1} & \tilde{p}_{I,2} & \cdots & \tilde{p}_{i,I} \end{bmatrix} \end{array} \tag{13}$$

Then, the relative importance values $\tilde{p}_{x,y}$ are utilized in Equation (14) to obtain the synthetic extent value $\tilde{S}_{i=1,2,\ldots,I}$ of criteria $C_{i=1,2,\ldots,I}$ [45].

$$\tilde{S}_{i=1,2,\ldots,I} = \sum_{n=1}^{I} \tilde{p}_{i,n} \bigodot \left[\sum_{i=1}^{I} \sum_{n=1}^{I} \tilde{p}_{i,n} \right]^{-1} \quad i = 1, 2, \ldots, I \tag{14}$$

Afterwards, the total integral value with the index of optimism $I_T^{\propto}(\tilde{S}_{i=1,2,\ldots,I})$ [32,46–48] is used in Equation (15) to calculate the weight set $W = \{w_1, w_2, \ldots, w_I\}$.

$$w_i = \frac{I_T^{\propto}(\tilde{S}_i)}{\sum_{n=1}^{I} I_T^{\propto}(\tilde{S}_n)} i = 1, 2, \cdots, I \tag{15}$$

B. The expert evaluation starts with the fuzzification of the criteria $C_{i=1,2,\ldots,I}$. $J = 5$ linguistic labels are associated with membership functions $\mu_{C_{i,j}}(z_i) \mid j = 1, 2, \ldots, J$, where $z_i \in Z_i$ is the adjusted weather condition value at the checkpoint under analysis, and Z_i is its universe of discourse. The membership functions $\mu_{C_{i,j}}(z_i) \mid j = 1, 2, \ldots, J$ are used to fuzzify each criterion C_i. In this way, each fuzzified criterion is defined as $\tilde{C}_i = \left\{\mu_{C_{i,1}}(z_i), \cdots, \mu_{C_{i,5}}(z_i)\right\}$.

Afterwards, the fuzzified criteria vectors $\tilde{C}_{i=1,2,\ldots,I}$ are gathered in the fuzzy criteria matrix $\tilde{C}$, as shown in Equation (16). Each element $c_{i,j}$ of matrix $\tilde{C}$ represents a membership function $\mu_{C_{i,j}}(z_i)$. The rows of the fuzzy criteria matrix $\tilde{C}$ are a combination of the membership values of criteria $\tilde{C}_{i=1,2,\ldots,I}$.

$$\tilde{C} = \begin{bmatrix} c_{1,1} & \cdots & c_{1,J} \\ \vdots & \ddots & \vdots \\ c_{I,1} & \cdots & c_{I,J} \end{bmatrix} \tag{16}$$

After obtaining the fuzzy criteria matrix $\tilde{C}$, weighting is developed to assign greater relevance to those criteria that are more important. Subsequently, the weight set $W = \{w_1, w_2, \ldots, w_I\}$ obtained in FAHP is used to weight elements $c_{i,j}$ of fuzzy criteria matrix $\tilde{C}$, as defined in Equation (17). All weighted elements $c_{i,j}^w$ are combined in the fuzzy weighted criteria matrix $\tilde{C}^w$ shown in Equation (18).

$$c_{i,j}^w = c_{i,j} * w_i \tag{17}$$

$$\tilde{C}^w = \begin{bmatrix} c_{1,1}^w & \cdots & c_{1,J}^w \\ \vdots & \ddots & \vdots \\ c_{I,1}^w & \cdots & c_{I,J}^w \end{bmatrix} \tag{18}$$

The next step of the expert evaluation is the selective assessment, which is responsible for modeling the relationships among the fuzzy weighted criteria $c_{i,j}^w$. However, the selective assessment determines the criteria $c_{i,j}^w$, which are relevant for the assessment of each alternative A_k [32].

Furthermore, the selective assessment defines a set of evaluations $E^k = \left\{e_1^k, e_2^k, \ldots, e_{N_k}^k\right\}$, which contains the result $e_{n=1,2,\ldots,N_k}^k$ defined in Equation (19). The number of evaluations $N_{k=1,2,\ldots,K}$ is resolved by the decision makers according to the fuzzy weighted criteria $c_{i,j}^w$ selected for the assessment of each alternative $A_{k=1,2,\ldots,K}$.

$$e_{n=1,2,\ldots,N}^k = f^k(n, \tilde{C}^w) \tag{19}$$

where the selective assessment function $f^k(n, \tilde{C}^w) \mid n = 1, 2, \ldots, N_k$, defined in Equation (20), assesses the fuzzy weighted criteria $c_{i,j}^w \epsilon \tilde{C}^w$ selected for the evaluations $e_{n=1,2,\ldots,N_k}^k$ of alternative $A_{k=1,2,\ldots,K}$.

$$f^k(n, \tilde{C}^w) = \min\left(D_n^k = \left\{d_{i,j}^k \middle| i = 1, 2, \ldots, I; j = 1, 2, \ldots, J\right\}\right) \tag{20}$$

in which the elements $d_{i,j}^{k}$ of the relationship modeling matrix D_{n}^{k} determine whether a fuzzy weighted criterion $c_{i,j}^{w}$ is used ($d_{i,j}^{k} = c_{i,j}^{w}$) or not used ($d_{i,j}^{k} = 1$) in the assessment n of alternative A_k. Moreover, the relationship modeling matrix, defined by the decision makers, depends on the relationships among the weather conditions, the spatial features of the checkpoint, the crop features, and the soil moisture content.

After assessing the whole set E^k, the best assessment for each alternative A_k is obtained with Equation (21).

$$a_k = max\left(E^k\right) \tag{21}$$

Once the best assessments a_k are obtained for every alternative A_k, they are combined in a matrix $\begin{bmatrix} a_1 & \cdots & a_K \end{bmatrix}^T$. The best choice is achieved through Equation (22).

$$\hat{\mathrm{A}} = \max\left(\begin{bmatrix} a_1 \\ \vdots \\ a_K \end{bmatrix}\right) \tag{22}$$

C. Fuzzy inference: As FEADM does not only select a qualitative value (soil moisture level) but can also estimate a qualitative value (soil moisture value), a fuzzy inference process is included in the second stage.

An output membership function $\mu_{A_{k=1,2,\ldots,K}}$ is defined for each alternative A_k, as in [32]. Moreover, the best assessment a_k determines the maximum value for each output membership function $\mu_{A_{k=1,2,\ldots,K}}$; in this way, the actual output membership function $\mu_{A_k}^{*}$ is obtained, as shown in Equation (23).

$$\mu_{A_k}^{*} = \begin{cases} \mu_{A_k}; & \mu_{A_k} < a_k \\ a_k; & \mu_{A_k} \geq a_k \end{cases} \tag{23}$$

Then, the function μ_{Sm_e} is obtained using Equation (24). This function is utilized in the centroid method, shown in Equation (25). As a result, the soil moisture estimates Sm^r at checkpoint P^r are achieved.

$$\mu_{Sm_e} = \max\left(\mu_{A_1}^{*}, \mu_{A_2}^{*}, \cdots, \mu_{A_5}^{*}\right) \tag{24}$$

$$Sm^r = \frac{\sum_{l=0}^{L} \mu_{Sm_e}(z_{sm})_l z_l}{\sum_{l=0}^{L} \mu_{Sm_e}(z_{sm})_l} \tag{25}$$

2.3. Regional Estimation (Point Estimates of Soil Moisture)

The final result of FEADM, the second stage of the integrated approach, is a *point* estimate of the soil moisture. Additionally, in the integrated IWeCASF-FEADM approach, the set of checkpoints is scattered within a region, as in conventional systems. Thus, the soil moisture at these checkpoints must be determined. As a consequence, FEADM, which is responsible for obtaining the soil moisture, is executed at every checkpoint $P^{r=1,2,\ldots,R}$. Consequently, FEADM is implemented a total of R times, giving, as a result, soil moisture *point* estimates $Sm^{r=1,2,\ldots,R}$. The soil moisture *point* estimates $Sm^{r=1,2,\ldots,R}$ are combined in a set, which is named the *regional* soil moisture estimation $Re = \left\{Sm^1, Sm^2, \ldots, Sm^R\right\}$. If a more accurate *regional* soil moisture estimation is required, more checkpoints P^r must be defined to reduce the area without a *point* estimate.

3. Experimental Case Study

As presented above, the *regional* soil moisture estimation $Re = \left\{Sm^1, Sm^2, \ldots, Sm^R\right\}$ is a set of soil moisture *point* estimates $Sm^{r=1,2,\ldots,R}$, obtained based on two stages. The first stage is IWeCASF, which is necessary to supply the weather conditions $C_{i=1,2,\ldots,I}^{r}$ to FEADM, and the second stage is the integrated approach, IWeCASF-FEADM.

3.1. Inputs

As described in Section 2.1 and [39], the satellite imagery of the estimation region is divided into $S = 2150$ sectors $s(x, y)$. The total number of sectors, $S = 2150$, is determined from the experimental results so that the extension of each sector $s(x, y)$ is $40x40$ m. The estimation region is part of a basin with a length of almost 2 km. The different areas (grassy, tree-covered, and building areas) within the estimation region make it suitable for the exploration of diverse spatial features.

The satellite image in Figure 3 depicts the region of interest, the locations $s(x_r, y_r)$ of some checkpoints P^r and the feature matrix M^2 (crop type). As described in [39] and Section 3.1, the feature matrices M^t are given in the input soil and crop zones. The feature matrix M^2 is composed of elements $(m^1_{x,y})_{XxY}$. In this case, the feature matrix M^2 denotes two different crop types. The crop type influences the soil moisture estimation approach utilized in the integrated IWeCASF-FEADM approach.

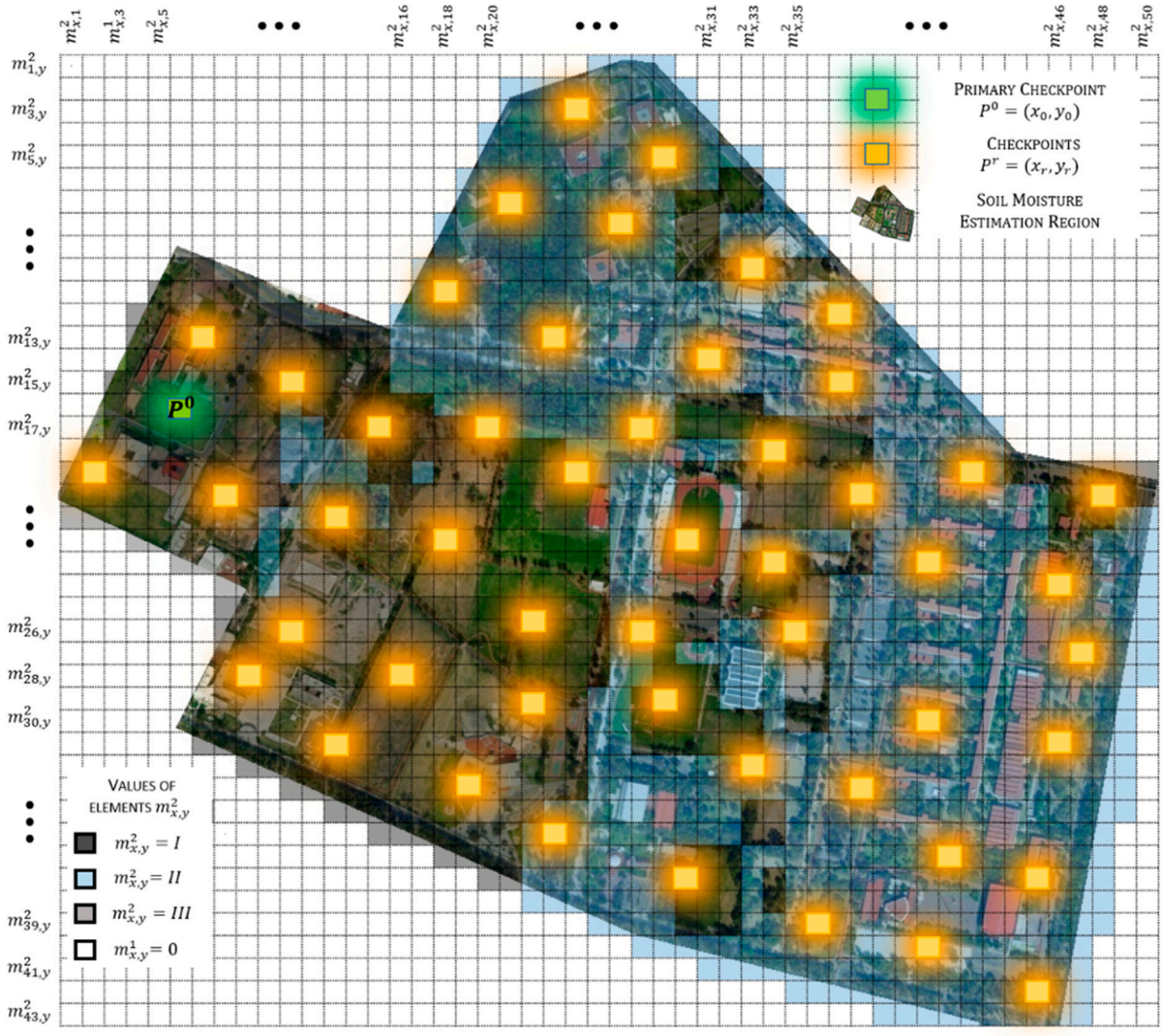

Figure 3. Feature matrix $M^{t=2}$ (crop type).

Additionally, with the integrated IWeCASF-FEADM approach, there can be as many checkpoints P^r as required, because this approach does not require the physical deployment of measurement equipment to obtain the soil moisture. Therefore, the more checkpoints there are, the more accurate the soil moisture estimation is, because fewer sectors $(x,)$ remain without a soil moisture estimate. In this experiment, each sector $s(x, y)$ is considered a checkpoint. The irrigation water matrix δ_{x_r, y_r} is utilized to complement the rain

record and corresponds to the irrigation water supplied at each sector $s(x, y)$ within the estimation region.

Moreover, IWeCASF [39], the first stage of the integrated approach, requires the weather conditions measured $C^0_{i=1,2,\ldots,I}$ at a single checkpoint (primary checkpoint P^0), which can also be identified in Figure 3. The weather condition $C^0_{i=1,2,\ldots,I}$ and values $v_{i=1,2,\ldots,I}$ used in this experiment are presented in Table 2 and are in line with [39].

Table 2. Weather conditions (measured) at the primary checkpoint P^0.

$C^0_{i=1,2,\ldots,I}$	Weather Condition	Value (v_i)
C^0_1	Temperature (°C)	19
C^0_2	Rain (mm)	5.8
C^0_3	Solar radiation (Wm^{-2})	265
C^0_4	Wind speed (kmh^{-1})	13
C^0_5	Evapotranspiration (mm)	3.28

3.2. Applying the IWeCASF-FEADM Integrated Approach

3.2.1. IWeCASF

IWeCASF processes the input satellite imagery to determine the landscape feature matrices F^l. Then, the feature matrices M^t, which are given as input, as well as the landscape feature matrices F^l, are used to determine the particular features $\mathbf{\Phi}^r\left(F^l, M^t, P^r\right)$ at a checkpoint P^r. Next, two adjustment factors for the weather conditions are obtained from two fuzzy inference systems. The first is the steady adjustment $\alpha_{r,i}$ determined by processing the influence of particular features $\mathbf{\Phi}^r\left(F^l, M^t, P^r\right)$ over the weather conditions $C^r_{i=1,2,\ldots,I}$. The second is the variable adjustment B, which is the result of modeling the interactions among weather conditions $C^r_{i=1,2,\ldots,I}$. Later, the steady adjustment $\alpha_{r,i}$ and the variable adjustment B are used to establish the weather conditions $C^r_{i=1,2,\ldots,I}$ at checkpoint P^r, which is called the final adjustment. The two stages (A and B) are described as follows:

A. Landscape features: As described in Section 2.2.1 A, B, the landscape features are extracted from the satellite imagery; then, the landscape features of the checkpoint under review are selected for further analysis.

Firstly, a color space conversion is performed. The image of the estimation region is taken from the RGB color space, as shown in Figure A1a, to the CIELAB color space. Afterwards, the converted image is decorrelated; in this way, the prototype clusters $K_{l=1,2,\ldots,L}$ are more distinguishable. The prototype clusters $K_{l=1,2,\ldots,L}$ are required to perform image segmentation using the objective function G, as defined in Equation (1). Therefore, a more discernible prototype cluster $K_{l=1,2,\ldots,L}$ encourages better image segmentation. Figure A1b presents the decorrelated image of the estimation zone. As described in [39], in Figure A1b, tree-covered areas are shown in blue, buildings are shown in pink, and grasslands are shown in green, while they appear yellow when the grass is dry. Moreover, in Figure A1b, the prototype clusters $K_{l=1,2,3}$, which are used to define the landscape feature matrices $F^{l=1,2,3}$, are shown. The color segmentation utilizes a merge algorithm to assign each pixel of the image to a prototype cluster k_l.

After performing the color segmentation of the estimation zone image, the original image is separated into $L = 5$ landscape feature matrices $F^{l=1,2,\ldots,L}$, whose elements $f^l_{x,y}$ contain the number of pixels of sector $s(x, y)$ that belong to landscape feature l. In Figure 4, the landscape feature matrix $F^{l=2}$ (tree-covered area) is depicted. Furthermore, a magnified image of sector $s(22, 26)$ is presented to illustrate the element $f^2_{22,26} = 48$, i.e., there are 48 of a total of 156 pixels that belong to landscape feature $l = 2$ at sector $s(22, 26)$.

After determining the landscape feature matrices $F^{l=1,2,\ldots,L}$, the next step is selecting the particular features at a checkpoint. As mentioned previously, every sector within the estimation region can be considered a checkpoint; thus, the checkpoint P^r under consideration in the experiment described in this section is the sector $s(22, 26)$. In this

way, using Equations (2) and (3), the particular feature vector $\mathbf{\Phi}^r\left(F^t, M^t, P^r\right)$ at checkpoint $P^r = s(22, 26)$ is as presented in Equations (26) and (27), and they are depicted in Figure 5.

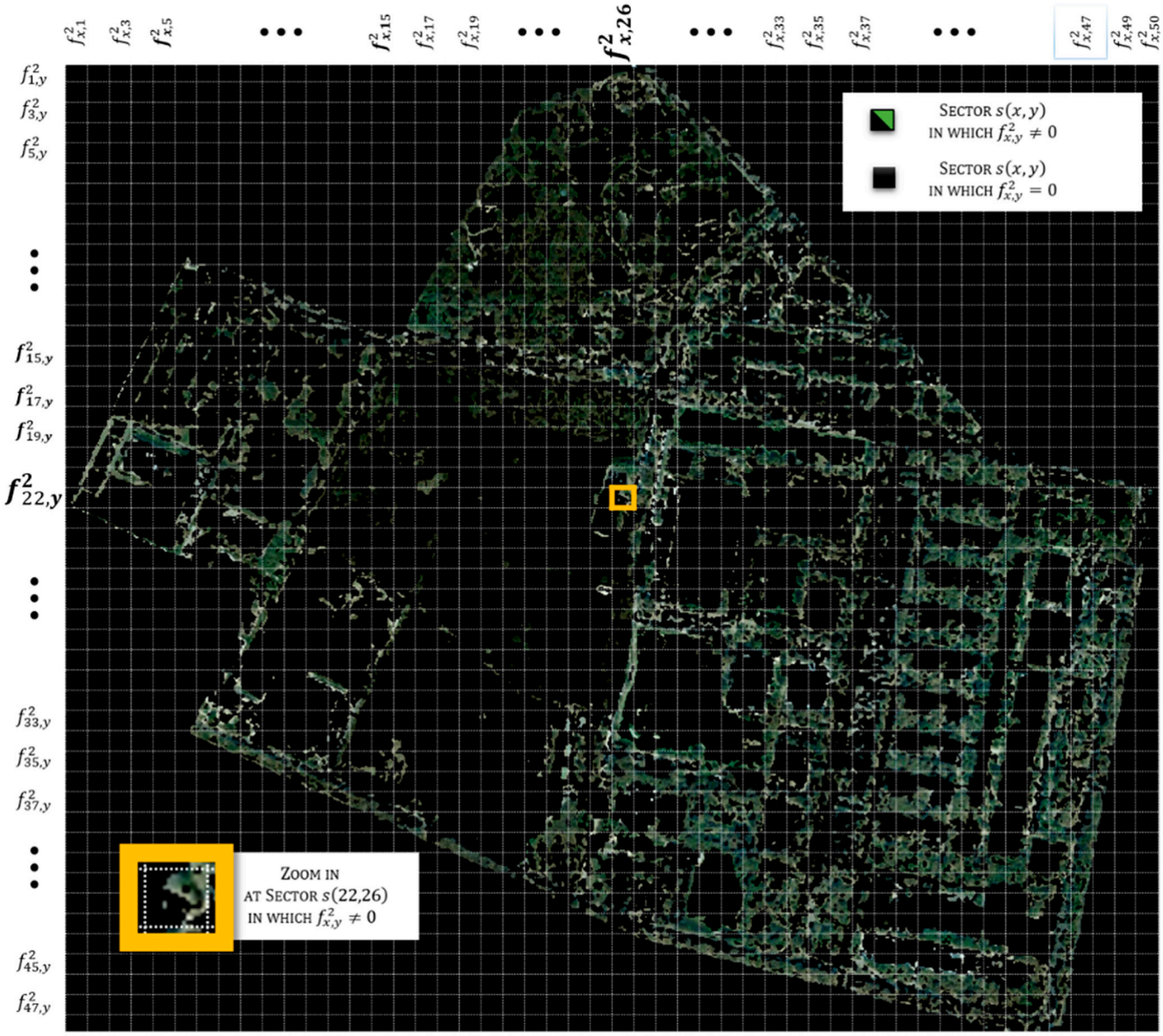

Figure 4. Landscape feature matrix F^2 (tree-covered area).

In Equation (26), the particular feature vector $\mathbf{\Phi}^r\left(F^l, M^t, P^r\right)$ is expressed as a number of pixels; for example, there are 21 pixels that belong to landscape feature $l = 1$ (grassland), and 69 pixels belong to landscape feature $l = 3$ (buildings). Furthermore, the particular feature vector $\mathbf{\Phi}^r\left(F^l, M^t, P^r\right)$ is expressed as a percentage in Equation (27); for example, 65.38% of the pixels at the checkpoint $P^r = s(22, 26)$ correspond to $l = 1$ (grassland), and 35.1% of the pixels belong to $l = 3$ (buildings).

$$\mathbf{\Phi}^r\left(F^l, M^t, P^r\right) = [21, 105, 69, (196/A), 574, (196/II), (196/1), (196/1)] \quad (26)$$

$$\mathbf{\Phi}^r\left(F^l, M^t, P^r\right) = [65.38, 53.57, 35.1, (100/A), 35.2, (100/II), (100/1), (100/1)] \quad (27)$$

B. Weather condition adjustment: As explained previously, there are two adjustment factors for the weather conditions. The first is derived from steady adjustment, which

analyzes the landscape features of the estimation region and their influence over the weather conditions. The second is obtained from variable adjustment, which considers the interactions between the weather conditions.

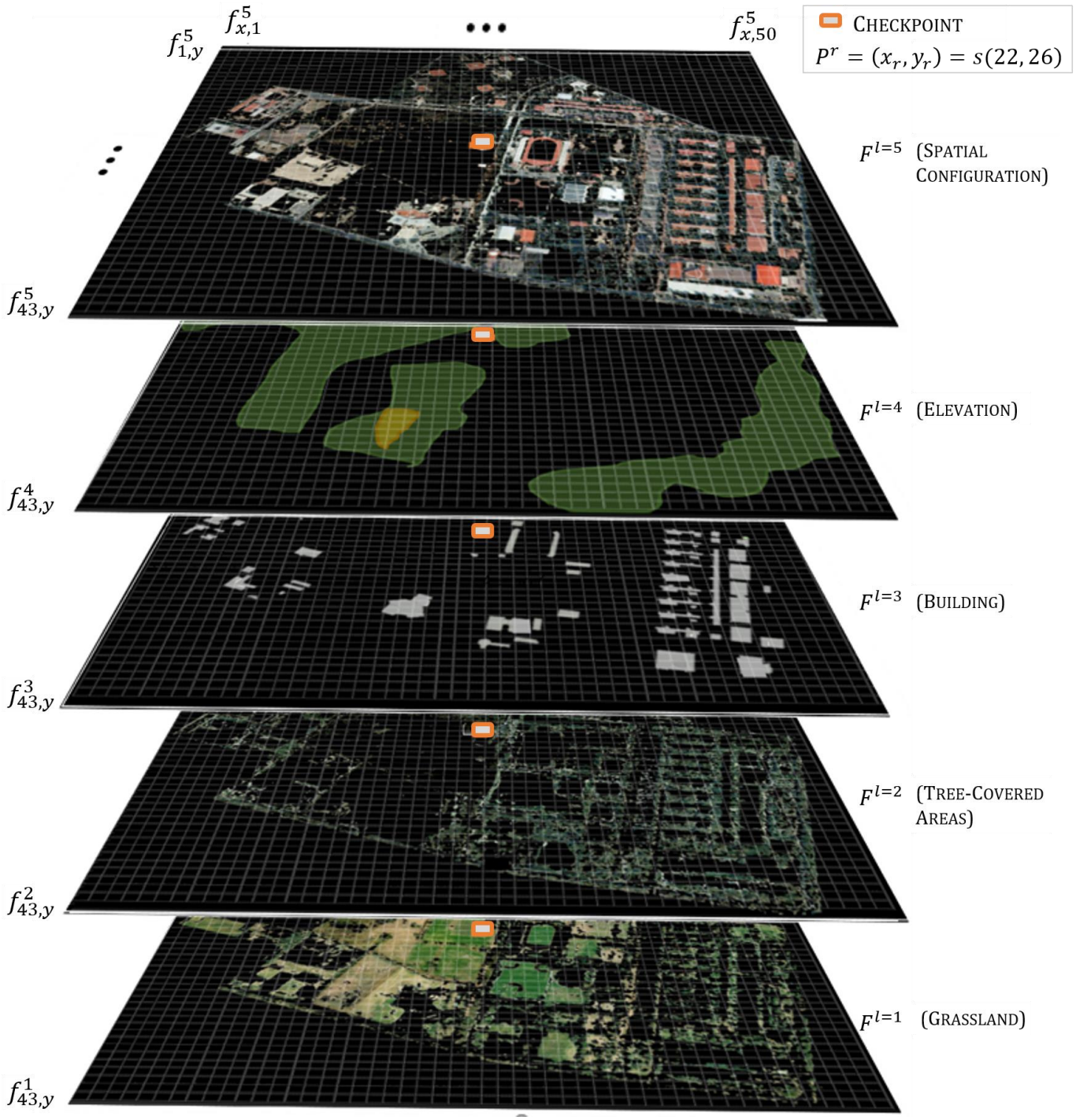

Figure 5. Landscape feature matrices $F^{l=1,2,\ldots,5}$.

The steady and variable adjustments are developed using a fuzzy inference system (FIS). For this reason, a fuzzification stage is performed. According to Equations (4)–(8), the weather conditions $C^0_{i=1,2,\ldots,I}$ are measured at the primary checkpoint P^0.

Five membership functions ($J = 5$) are defined to fuzzify each weather condition, as in [39]; the parameters used to fuzzify the weather conditions $C^0_{i=1,2,\ldots,I}$ and their actual

values are also described in [39]. The resulting fuzzy weather condition vectors $\tilde{C}_i^0(v_i)$ are shown in Equations (28)–(32).

$$\tilde{C}_1^0(19.5) = \{0, 0, 0.9, 0, 0\} \quad | \text{ Temperature} \tag{28}$$

$$\tilde{C}_2^0(5.8) = \{0, 0, 0.0909, 0.2667, 0\} \quad | \text{ Rain} \tag{29}$$

$$\tilde{C}_3^0(265) = \{0, 0, 0.25, 0, 0\} \quad | \text{ Solar radiation} \tag{30}$$

$$\tilde{C}_4^0(13) = \{0, 0, 0.6, 0, 0\} \quad | \text{ Wind speed} \tag{31}$$

$$\tilde{C}_5^0(3.28) = \{0, 0, 0.98, 0, 0\} \quad | \text{ Evapotranspiration} \tag{32}$$

Moreover, a comparison $\mathbf{\Phi}^{0,r}$ between the particular features $\mathbf{\Phi}^r\left(F^l, M^t, P^r\right)$ at checkpoint P^r and the particular features $\mathbf{\Phi}^0\left(F^l, M^t, P^0\right)$ at the primary checkpoint P^0 is performed using Equation (9); this is shown in Equations (33) and (34) and finally in Equation (35). The particular feature comparison $\mathbf{\Phi}^{0,r}$ is intended to assess the weather condition disparities regarding a variation in the landscape features.

$$\mathbf{\Phi}^0\left(F^l, M^t, P^0\right) = [100, 0, 0, (100/A), 22.76, (100/II), (100/1), (100/1)] \tag{33}$$

$$\begin{aligned}\mathbf{\Phi}^{0,r} = {} & 100 - 10.2, 0 - 53.2, 0 - 35.1, (100 - 100)/A, 22.76 - \\ & 35.6, (100 - 100)/I, (100 - 100)/1, (100 - 100)/1\end{aligned} \tag{34}$$

$$\mathbf{\Phi}^{0,r} = [89.8, -53.2, -35.1, (0/A), 12.84, (0/I), (0/1), (0/1)] \tag{35}$$

Afterwards, the fuzzy particular feature matrix $\tilde{\mathbf{\Phi}}^r$, shown in Equation (36), is derived by fuzzifying the comparison $\mathbf{\Phi}^{0,r}$ presented in Equation (35) according to Equation (10). The resulting fuzzy particular feature matrix $\tilde{\mathbf{\Phi}}^r$ presented in Equation (36) shows the great similarity between primary checkpoint P^0 and checkpoint P^r; as a result, a barely significant weather condition adjustment is expected at checkpoint P^r.

$$\tilde{\mathbf{\Phi}}^r = \begin{bmatrix} 0 & 0 & 1 \\ 0.9388 & 0 & 0 \\ 0.2812 & 0.125 & 0 \\ 0 & 1 & 0 \\ 0 & 0.68 & 0 \\ 0 & 1 & 0 \\ 0 & 1 & 0 \\ 0 & 1 & 0 \end{bmatrix} \tag{36}$$

As defined in [39], the steady adjustment FIS utilizes **IF THEN** rules as the form of the rule $n = 23$, which is described as follows:

- **IF** the grassland is high $(\tilde{\phi}_{1,2}^r)$, the tree cover area is equal $(\tilde{\phi}_{2,2}^r)$, the building area is less $(\tilde{\phi}_{3,1}^r)$, the elevation is equal $(\tilde{\phi}_{4,2}^4)$, and the spatial configuration is less $(\tilde{\phi}_{5,2}^r)$, **THEN** the adjustment factor for the temperature $(\alpha_{4,1})$ is null $(\lambda_{1,4})$, the adjustment factor for rain $(\alpha_{4,2})$ is null $(\lambda_{2,3})$, the adjustment factor for solar radiation $(\alpha_{4,3})$ is barely high $(\lambda_{3.4})$, the adjustment factor for the wind speed $(\alpha_{4,4})$ is null $(\lambda_{4,3})$, and the adjustment factor for evapotranspiration $(\alpha_{4,5})$ is barely high $(\lambda_{5,4})$.

After assessing the $N = 245$ rules as described in [39] and Section 3.2.1 B, the result is the steady adjustment factor $\alpha_{r,i}$, presented as the vector $\Lambda_r = (\alpha_{r,i})_{1,I}$, shown in Equation (37). For example, the adjustment factor for solar radiation $\alpha_{r,3}$ shows that, at checkpoint P^r, the solar radiation adjustment factor is approximately $+4.99\%$ of its value.

$$\Lambda_r = [-0.0288, -0.003, -0.0499, -0.225, -0.288] \tag{37}$$

Moreover, the certainty of the weather condition replication $\eta_{i=1,2,\ldots,I}$ improves the modeling of inconsistent weather conditions, as described in Section 3.2.1 B. According to [39], the certainty $\eta_{i=1,2,\ldots,I}$ is calculated with a distribution function. Then, the variable adjustment is developed to determine the second adjustment factor. In the same way as for the steady adjustment FIS, a set of **IF THEN** rules is utilized. However, in the variable adjustment, $Q = 445$ rules are assessed; for example, the following rule corresponds to $q = 412$.

- **IF** the temperature is high $\left(\tilde{c}^0_{1,4}\right)$ **and** rain is low $(\tilde{c}^0_{2,2})$ **and** solar radiation is higher $\left(\tilde{c}^0_{3,5}\right)$ **and** evapotranspiration is higher, **THEN** outputs β_1, β_5, β_2 β_3, β_4 are equal $(\omega_{1,3}, \omega_{2,3}, \omega_{3,3}, \omega_{4,3}, \omega_{5,3})$.

The variable adjustment factor B is unique for the whole estimation region. In Equation (38), the adjustment factor B resulting from the variable adjustment of the weather conditions $C^0_{i=1,2,\ldots,I}$ is presented. For example, the variable adjustment factor for rain β_2 is -0.0167, which means that there is an adjustment of -1.67% in the rain C^0_2.

$$B = [0, -0.0167, -0.0498, -0.0498, -0.0214] \tag{38}$$

Finally, IWeCASF determines the weather conditions at the checkpoint P^r by using Equation (11), where the steady adjustments $(\alpha_{r,i})_{1,I}$ and variable B, which are obtained in Equations (37) and (38), are utilized. The resulting adjusted weather conditions $C^r_{i=1,2,\ldots,I}$ are shown in Table 3. The value of rain is $C^0_2 = 5.8$, and its adjustment factors are $\alpha_{r,1} = -0.003$ and $\beta_2 = -0.0167$, according to Equations (37) and (38). As a consequence, the measured value $C^0_2 = 5.8$ is decreased in a combined factor of $-0.3\% - 1.67\% = -1.97\%$ of the measured value. Thus, the adjusted value of rain is $C^r_2 = 5.68$.

Table 3. Weather condition comparison at checkpoint P^4.

Weather Condition		Adjusted Ca^4_i	Measured Cm^4_i
$i = 1$	Temperature (°C)	18.93	19.5
$i = 2$	Rain (mm)	5.68	5.8
$i = 3$	Solar radiation (W m^{-2})	238.57	265
$i = 4$	Wind speed (Km h^{-1})	9.42	13
$i = 5$	Evapotranspiration (mm)	2.62	3.8

3.2.2. Irrigation Water Addition

Afterwards, the weather conditions $C^r_{i=2}$ are applied, as shown in Equation (12), with the irrigation water record δ_{x_r,y_r} at checkpoint P^r. In this experiment, the irrigation water record δ_{x_r,y_r} at checkpoint P^r is $\delta_{x_r,y_r} = 4.12$. Therefore, according to Equation (12), the actual weather conditions $\check{C}^r_{i=1,3,4,5}$ are the same as the weather conditions given in Table 3, as shown in Equations (39) and (41)–(43); meanwhile, the actual weather condition $\check{C}^r_{i=2}$ is calculated using Equation (40). They are introduced to FEADM.

$$\check{C}^r_{i=1} = C^r_1 = 18.93 \quad | \text{ Temperature} \tag{39}$$

$$\check{C}^r_{i=2} = C^r_2 + \delta_{x_r,y_r} = 5.8 + 4.12 = 9.92 \quad | \text{ Rain} \tag{40}$$

$$\check{C}^r_{i=3} = C^r_3 = 238.57 \quad | \text{ Solar radiation} \tag{41}$$

$$\check{C}^r_{i=4} = C^r_4 = 9.42 \quad | \text{ Wind speed} \tag{42}$$

$$\check{C}^r_{i=5} = C^r_5 = 2.62 \quad | \text{ Evapotranspiration} \tag{43}$$

3.2.3. FEADM

The second stage of the integrated approach is the "fuzzy estimation approach based on decision making" (FEADM) [32]. Unlike IWeCASF [39], which is performed only one time for each regional estimation *Re*, FEADM is executed as many times as there are checkpoints P^r. FEADM is implemented to obtain a soil moisture *point* estimate Sm^r at each checkpoint P^r. Consequently, FEADM receives as inputs the actual weather conditions $\check{C}^r_{i=1,2,\ldots,I}$ at checkpoint P^r, obtained from IWeCASF in the previous stage of the integrated approach. Then, FEADM determines the soil moisture level that best fits the current weather conditions. Afterwards, a quantitative value of the chosen soil moisture level is obtained. This quantitative value is the soil moisture *point* estimate Sm^r at checkpoint P^r. The two stages (A and B) are described as follows:

A. FEADM decision-making stage: This begins with the fuzzy analytical hierarchy process (FAHP), as described in [32] and Section 3.2.3 A. In this stage, the criteria C_i are compared to obtain the judgment matrix $\tilde{P}$ defined in Equation (44). Each element $\tilde{p}_{x,y}$ of judgement matrix $\tilde{P}$ denotes the relevance of criteria C_x regarding criteria C_y. The assignment of the relative importance values is performed as in [32].

$$\tilde{P} = \begin{array}{c} \\ C_1 \\ C_2 \\ C_3 \\ C_4 \\ C_5 \end{array} \begin{array}{c} \begin{array}{ccccc} C_1 & C_2 & C_3 & C_4 & C_5 \end{array} \\ \begin{bmatrix} (1,1,1) & (1,1,1) & (1,2,3) & (1,2,3) & (1,2,3) \\ (1,1,1) & (1,1,1) & (2,4,6) & (4,6,8) & (4,6,8) \\ \left(\frac{1}{3},\frac{1}{2},1\right) & \left(\frac{1}{3},\frac{1}{2},1\right) & (1,1,1) & (4,6,8) & (1,2,3) \\ \left(\frac{1}{3},\frac{1}{2},1\right) & \left(\frac{1}{8},\frac{1}{6},\frac{1}{4}\right) & \left(\frac{1}{8},\frac{1}{6},\frac{1}{4}\right) & (1,1,1) & (1,1,1) \\ \left(\frac{1}{3},\frac{1}{2},1\right) & \left(\frac{1}{8},\frac{1}{6},\frac{1}{4}\right) & \left(\frac{1}{3},\frac{1}{2},1\right) & (1,1,1) & (1,1,1) \end{bmatrix} \end{array} \quad (44)$$

Afterwards, the extent of synthetic values $\tilde{S}_{i=1,2,\ldots,I}$ is calculated with Equation (13), as in [32]. Furthermore, the total integral value with the index of optimism $I^{\propto}_T\left(\tilde{S}_{i=1,2,\ldots,I}\right)$ and the extent of synthetic values $\tilde{S}_{i=1,2,\ldots,I}$ are used in Equation (14) to obtain the weight set W, which is shown in Equation (45). According to Equation (45), the most relevant criterion is rain (C_2), as was expected.

$$W = \{0.1834, 0.3805, 0.2555, 0.0791, 0.1015\} \quad (45)$$

The FEADM decision-making stage continues with the expert evaluation. Firstly, the assessment criteria $C_{i=1,2,\ldots,I}$ are fuzzified, as performed in [32]. As shown in Table 3, the actual weather conditions $\check{C}^r_{i=1,2,\ldots,I}$ are utilized as assessment criteria $C_{i=1,2,\ldots,I}$. Thus, in this experiment, the values $\check{C}^r_{i=1,2,\ldots,I}$ shown in Equations (39)–(43) are the values z_i, which, in addition to the membership functions $\mu_{C_{i,j}}(z_i)$ defined in [32], are used to obtain the fuzzy criterion $\tilde{C}_i = \left\{\mu_{C_{i,1}}(z_i), \cdots, \mu_{C_{i,5}}(z_i)\right\}$. After fuzzifying the five criteria ($I = 5$), the fuzzy criteria matrix $\tilde{C}$ can be obtained using Equation (15). In this experiment, the resulting fuzzy criteria matrix $\tilde{C}$ is as shown in Equation (46).

$$\tilde{C} = \begin{bmatrix} 0 & 0.0333 & 0.36 & 0 & 0 \\ 0 & 0 & 0 & 0 & 1 \\ 0 & 0.6667 & 0 & 0 & 0 \\ 0 & 0 & 0.8 & 0 & 0 \\ 0 & 0.3 & 0 & 0 & 0 \end{bmatrix} \quad (46)$$

Next, the weight set W from Equation (45) and the fuzzy criteria matrix $\tilde{C}$ from Equation (46) are used in Equation (47) to calculate the elements of the fuzzy weighed criteria matrix $\tilde{C}^w$, shown in Equation (18). The $\tilde{C}^w$ resulting from this experiment is given in Equation (47).

$$\tilde{C}^w = \begin{bmatrix} 0 & 0.0061 & 0.066 & 0 & 0 \\ 0 & 0 & 0 & 0 & 0.385 \\ 0 & 0.1703 & 0 & 0 & 0 \\ 0 & 0 & 0.0633 & 0 & 0 \\ 0 & 0.0305 & 0 & 0 & 0 \end{bmatrix} \quad (47)$$

The fuzzy weighed criteria matrix $\tilde{C}^w$ is required in the selective assessment [32]. The number of assessments $N_{k=1,2,\ldots,K}$ used in this experiment is the same as defined in [32]. To accomplish each set of evaluations $E^k = \left\{e_1^k, e_2^k, \ldots, e_{N_k}^k\right\}$, according to Equations (19) and (20), the selective assessment function $f^k\left(n, \tilde{C}^w\right)$ evaluates the fuzzy weighted criteria $c_{i,j}^w$ defined in the relationship modeling matrix D_n^k, which only contains those $c_{i,j}^w$ relevant for evaluation e_n^k. The matrices $D_{n=1,2,\ldots,25}^5$ shown in Equations (48)–(50) correspond to alternative very high (A_5) instances; meanwhile, the matrices depicted in Equations (51)–(53) are three of the matrices used to assess alternative very low (A_1) instances. All matrices D_n^k presented in this experiment correspond to evaluations e_n^k performed at checkpoint $P^r = s(22, 26)$, as mentioned before. The matrices D_n^k are determined by the particular features $\phi^r\left(F^l, M^t, P^r\right)$ of the checkpoint P^r, where the evaluation e_n^k is conducted. Thus, given a checkpoint $P^{r=x}$ and a checkpoint $P^{r=y}$ with particular features $\phi^{r=x}\left(F^l, M^t, P^{r=x}\right) = \phi^{r=y}\left(F^l, M^t, P^{r=y}\right)$, the matrices D_n^k used to assess checkpoint $P^{r=x}$ can also be used to assess checkpoint $P^{r=y}$; i.e., if the spatial features of one or more checkpoints are the same, the assessment can be conducted using the same matrices D_n^k.

$$D_2^5 = \begin{bmatrix} 1 & 0.0061 & 1 & 1 & 1 \\ 1 & 1 & 1 & 1 & 0.385 \\ 1 & 1 & 1 & 1 & 1 \\ 1 & 1 & 1 & 1 & 1 \\ 1 & 0.0305 & 1 & 1 & 1 \end{bmatrix} \quad (48)$$

$$D_5^5 = \begin{bmatrix} 1 & 1 & 0.066 & 1 & 1 \\ 1 & 1 & 1 & 1 & 0.385 \\ 1 & 1 & 1 & 1 & 1 \\ 1 & 1 & 1 & 1 & 1 \\ 1 & 0.0305 & 1 & 1 & 1 \end{bmatrix} \quad (49)$$

$$D_{17}^5 = \begin{bmatrix} 1 & 1 & 0.066 & 1 & 1 \\ 1 & 1 & 1 & 0 & 1 \\ 0 & 1 & 1 & 1 & 1 \\ 1 & 1 & 1 & 1 & 1 \\ 1 & 0.0305 & 1 & 1 & 1 \end{bmatrix} \quad (50)$$

$$D_3^1 = \begin{bmatrix} 1 & 1 & 1 & 0 & 1 \\ 1 & 0 & 1 & 1 & 1 \\ 1 & 1 & 1 & 0 & 1 \\ 1 & 1 & 0.0633 & 1 & 1 \\ 1 & 1 & 1 & 1 & 0 \end{bmatrix} \quad (51)$$

$$D_{32}^1 = \begin{bmatrix} 1 & 1 & 1 & 0 & 1 \\ 0 & 1 & 1 & 1 & 1 \\ 1 & 1 & 0 & 1 & 1 \\ 1 & 1 & 1 & 1 & 1 \\ 1 & 1 & 1 & 0 & 1 \end{bmatrix} \quad (52)$$

$$D_{37}^{1} = \begin{bmatrix} 1 & 1 & 1 & 1 & 1 \\ 0 & 1 & 1 & 1 & 1 \\ 1 & 1 & 1 & 1 & 0 \\ 1 & 1 & 1 & 1 & 1 \\ 1 & 1 & 1 & 1 & 1 \end{bmatrix} \tag{53}$$

After assessing the N_k matrices $D_{n=1,2,\ldots,N_k}^{k}$ of each alternative A_k, the set of evaluations $E^k = \left\{e_1^k, e_2^k, \ldots, e_{N_k}^k\right\}$ is performed. The resulting sets E^k are of the form described in Equations (54) and (55), which correspond to sets E^1 and E^5 of very low (A_1) and very high (A_5) alternatives.

$$E^1 = \left\{e_n^1 = 0 \middle| n = 1, 2, \ldots, 37\right\} \tag{54}$$

$$E^5 = \left\{.0385, e_n^5 = 0 \middle| n = 2, 3, \ldots, 25\right\} \tag{55}$$

Afterwards, the best assessment a_k is obtained for each evaluation set $E^k = \left\{e_1^k, e_2^k, \ldots, e_{N_k}^k\right\}$ using Equation (22). The best assessment a_k of each alternative in this experiment is shown in Table 4.

Table 4. Best assessment a_k.

Soil Moisture Level	Alternative $A_{k=1,2,\ldots,K}$	Best Assessment $a_{k=1,2,\ldots,K}$
Very Low	A_1	0
Low	A_2	0
Medium	A_3	0
High	A_4	0.41
Very High	A_5	0

$A_1A_2A_3A_4A_5$ The FEADM decision-making stage ends with the selection of the best-assessed alternative $\hat{A}$, according to Equation (22) and Table 4. In this experiment, the best-assessed alternative $\hat{A}$ is high (A_4), as depicted in Equation (56).

$$\hat{A} = \max\left([0, 0, 0, 0.41, 0]^T\right) \tag{56}$$

Thus far, FEADM has determined that the soil moisture level high (A_4) is the best alternative according to the actual weather conditions ($\check{C}_{i=1,2,\ldots,I}^{r}$) at checkpoint P^r. Next, the crisp value of soil moisture Sm^r is calculated in the FEADM fuzzy inference stage.

B. Fuzzy inference: In the fuzzy inference proposed in [32], a membership function $\mu_{A_{k=1,2,\ldots,K}}(z_{sm})$ assigned to every alternative $A_{k=1,2,\ldots,K}$ is modified using the best assessment a_k of each alternative A_k, as shown in Equation (23); i.e., the actual output membership function $\mu_{A_k}^{*}(z_{sm})$ of alternative A_k is delimited by the best assessment a_k of the same alternative. For the soil moisture estimate Sm^r, the range $Z_{sm} = [0,\ 10]$ is defined considering the measurement range of the soil moisture sensor utilized. Finally, the soil moisture estimate Sm_e is obtained using Equation (24) for fuzzy aggregation and Equation (25) for defuzzification. The soil moisture estimate Sm^r at checkpoint P^r is shown in Equation (57).

$$Sm^r = 7.14 \tag{57}$$

3.3. Point Estimates of Soil Moisture

As depicted in Figure 2, when *regional* soil moisture estimation $Re = \left\{Sm^1, Sm^2, \ldots,\ Sm^R\right\}$ is conducted, IWeCASF, the first stage of the integrated approach, is completed only once, whereas FEADM, the second stage of the integrated approach, is performed as many times as required for soil moisture *point* estimate Sm^r. Furthermore, the previous analysis developed in Sections 3.2.1–3.2.3 has to be performed for every checkpoint P^r. As a result, a soil moisture *point* estimate is obtained at each sector $s(x, y)$.

Figure 6 illustrates the regional estimation $Re = \{Sm^1, Sm^2, \ldots, Sm^R\}$ of the area of interest. The irrigation water δ_{x_r,y_r} increases the soil water content. This is why irrigation water causes higher soil moisture levels in specific sectors ($9 \leq Sm < 10$). Moreover, there are areas in which the soil moisture estimation Sm is unavailable (N/A) due to the existence of buildings.

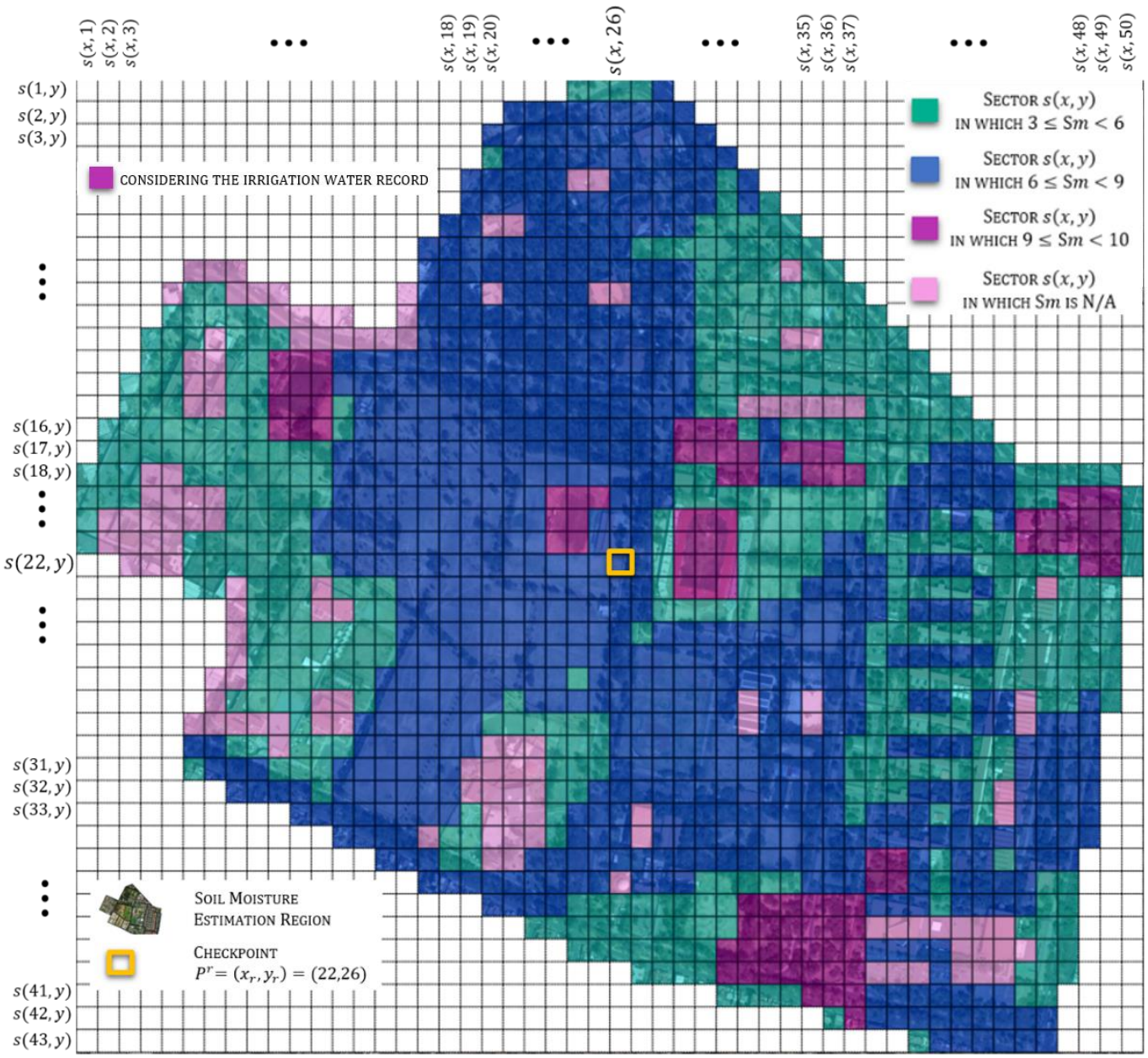

Figure 6. Soil moisture *regional* estimation $= \{Sm^1, Sm^2, \ldots, Sm^R\}$, considering irrigation water record δ_{x_r,y_r}, which increases soil water content.

4. Results and Discussion

The integrated approach based on linking FEADM with ICASF allowed *regional* soil moisture estimation, reducing the implementation and maintenance complexity of conventional automatic irrigation systems and their inherent costs. Although the experimental case study was for the region in Figure 1, this integrated approach can be applied in any estimation region with the required input data (satellite imagery, crop and soil data, weather conditions measured at a single checkpoint, and irrigation water record).

The method to obtain the *regional* soil moisture estimate combines two models published by our research team. In addition, it considers the irrigation water records, which were not previously used. The integrated approach is functional and has been tested for several years. The IWeCASF model [39] provides the required inputs for FEADM [32]. In the previous section, IWeCASF's results were complemented by the irrigation water records of the region of interest. However, if the irrigation water record is not considered and FEADM is applied, the results would be as depicted in Figure 7.

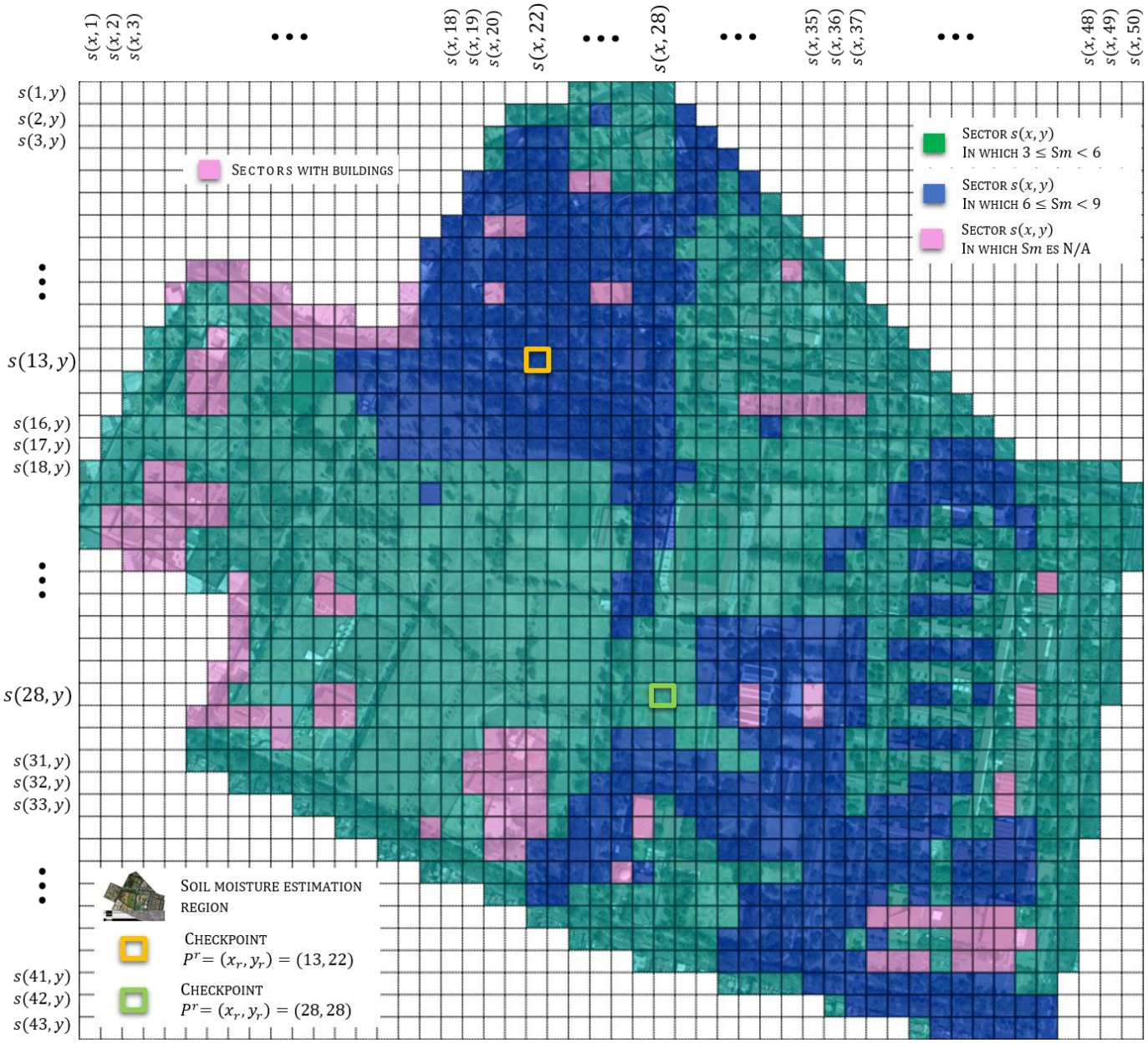

Figure 7. Soil moisture *regional* estimation $Re = \{Sm^1, Sm^2, \ldots, Sm^R\}$ without considering irrigation water record δ_{x_r,y_r}.

In this case, the soil moisture Sm^r is higher in mostly tree-covered checkpoints, such as the checkpoint at the sector $P^r = s(13,\ 22)$ with $Sm^r = 6.32$, compared to mainly grassland checkpoints, such as $P^r = s(28,\ 28)$, where the soil moisture content is $Sm^r = 5.09$. This is because tree-covered areas preserve more soil moisture when performing this test under the actual weather conditions. This fact can be relevant if the crop type is a fruit that is ripened on trees. Furthermore, it is worth noting that the integrated approach can be performed

without an irrigation water record. Therefore, if required, this integrated approach is suitable for the determination of soil moisture using only rain in sowing regions. Thus, the integrated approach's application is comprehensive.

The regional estimation $Re = \{Sm^1, Sm^2, \ldots, Sm^R\}$ is presented as a set of soil moisture *point* estimates Sm^r. In Figures 6 and 7, each sector $s(x, y)$ is a checkpoint P^r so that FEADM is executed at every sector $s(x, y)$ of the region of interest. In this way, the regional estimation $Re = \{Sm^1, Sm^2, \ldots, Sm^R\}$ is composed of $R = 1366$ *point* estimates $Sm^{r=1,2,\ldots,1366}$.

A total of 921 measured weather conditions $C^0_{i=1,2,\ldots,5}$ and the same number of irrigation water records Δ^r were utilized to develop the IWeCASF-FEADM integrated approach. A total of 645 records were used to improve the performance of the approach, whereas 276 records were assigned to validate it. These 921 records were collected over almost three years to test the soil moisture estimation approach, considering a wide range of irrigation and weather conditions.

The estimation errors of four checkpoints from the estimation region are presented in Figure 8. The graphs correspond to checkpoints $P^r = (17,\ 8)$, $P^r = (22,\ 26)$, $P^r = (14,\ 35)$, and $P^r = (33,\ 47)$. The estimations at checkpoint $P^r = (17,\ 8)$ are the most accurate; the normalized error E_{RMS} for this checkpoint is $E_{RMS} = 0.0361$. Meanwhile, the normalized error for checkpoint $P^r = (22,\ 26)$ is $E_{RMS} = 0.0479$; for checkpoint $P^r = (14,\ 35)$, the error is $E_{RMS} = 0.0519$, and, for checkpoint $P^r = (33,\ 47)$, the error is $E_{RMS} = 0.0544$.

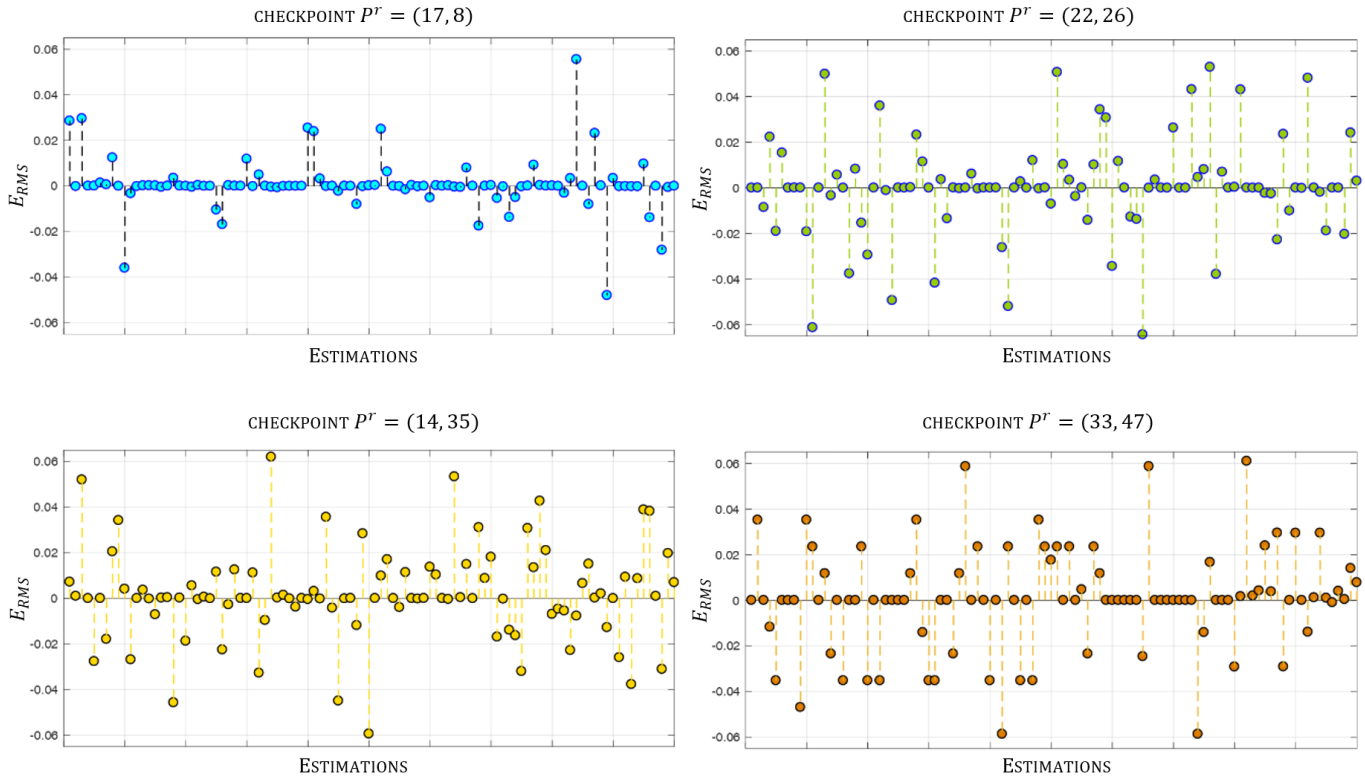

Figure 8. Soil moisture estimation error (E_{RMS}) for four checkpoints in the estimation region.

According to these results, and recalling the location of the primary checkpoint $P^0 = (16,\ 6)$, the performance of the integrated approach depends on the distance between the checkpoint P^r and the primary checkpoint P^0; i.e., the point estimate of soil moisture is more accurate when obtained closer to the checkpoint where the weather conditions $C^0_{i=1,2,\ldots,I}$ are measured.

Nevertheless, the results obtained at checkpoints that are distant from the primary checkpoint present a normalized error that does not imply a limitation in obtaining the soil moisture to determine the irrigation water supply.

Soil Moisture Behavior under Landscape Variability

The soil moisture is highly dependent on the landscape features and the weather conditions. An additional advantage of the method developed in this work (the integrated approach) is that it allows simulations to observe and verify these dependencies. In this sense, we simulate and present in Figure 9 the results when the landscape features F^t vary within a determined section of the estimation region. The influence of a change in a landscape feature F^t over the weather conditions $C^r_{i=1,2,\ldots,I}$ and soil moisture Sm^r is outstanding. A determined area (I, II, and III) of the region of interest is depicted. Each colored rectangle is a sector $s(x, y)$.

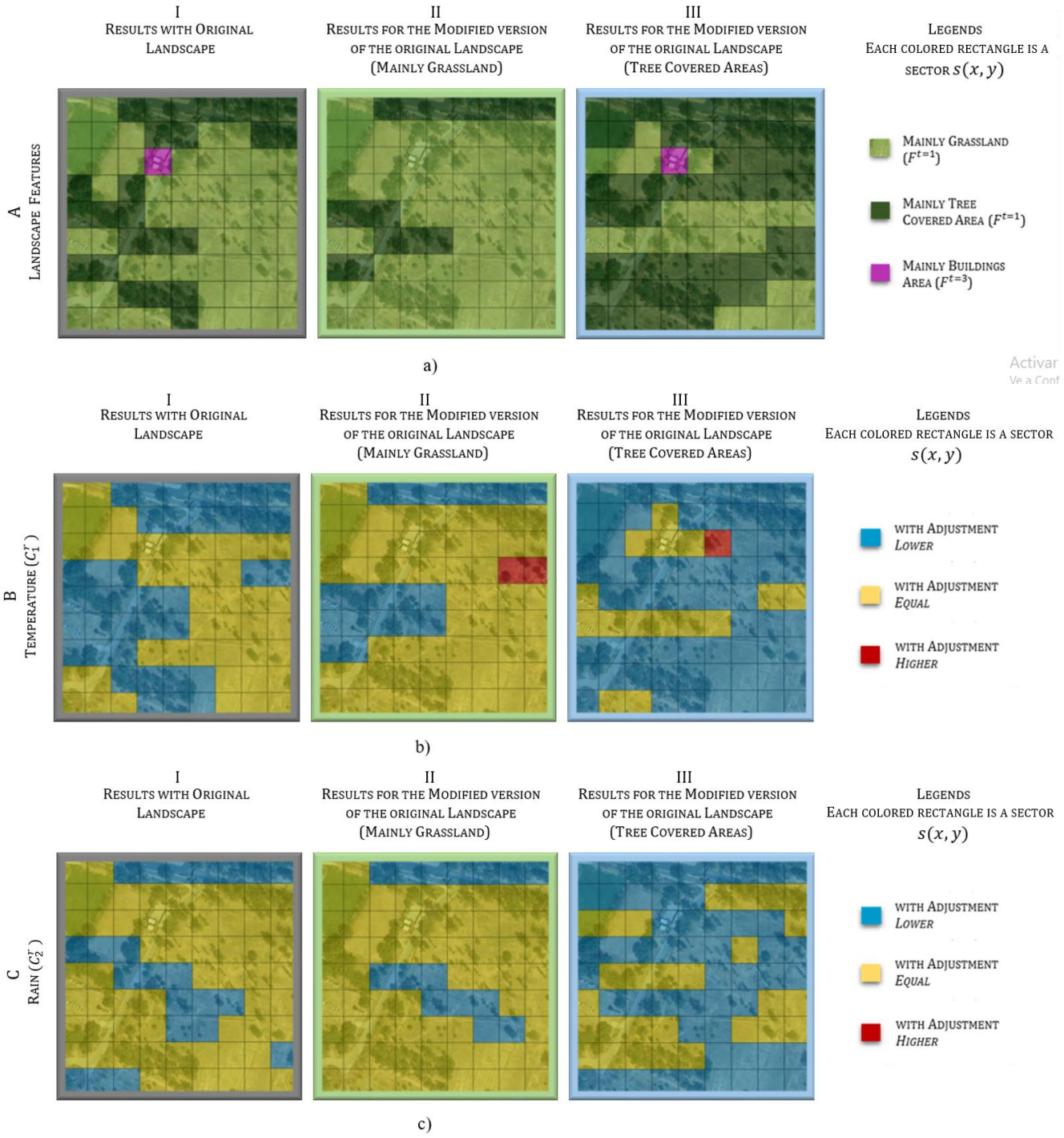

Figure 9. *Cont.*

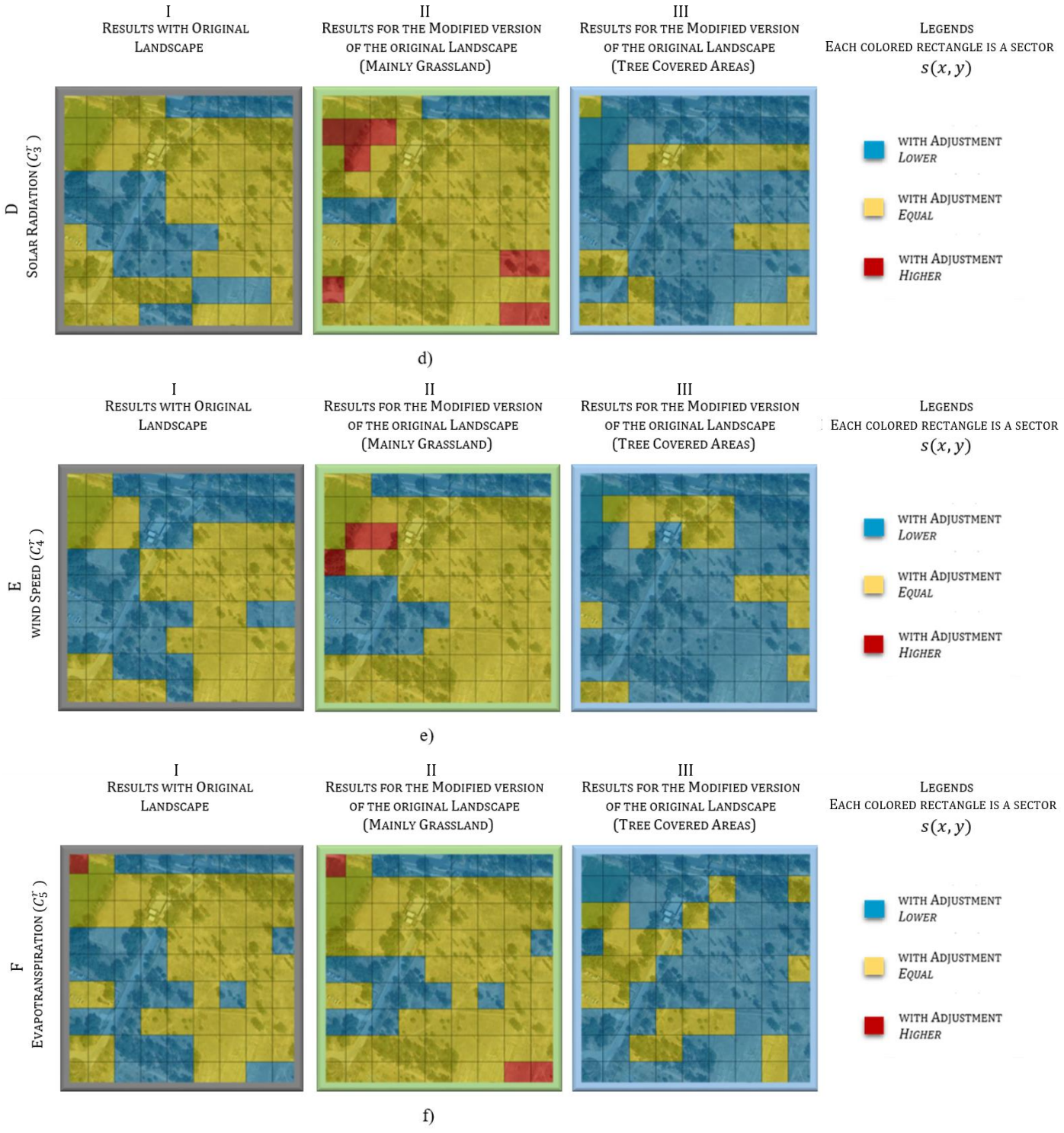

Figure 9. *Cont*.

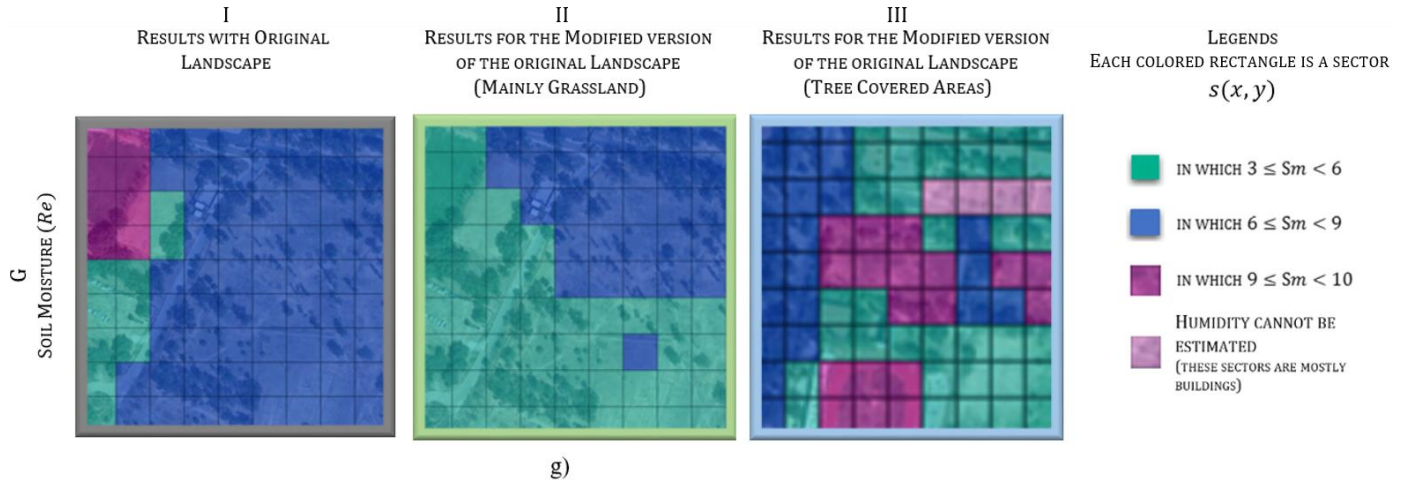

Figure 9. Landscape features F^t, weather conditions $C^r_{i=1,2,\ldots,I}$, and soil moisture Sm^r variability. (**a**) Changes in landscape features. (**b**–**f**) Weather conditions of temperature (C^r_1), rain (C^r_2), solar radiation C^r_3), wind speed C^r_4), and evapotranspiration (C^r_5) for each category: original landscape, grassland, and tree-covered areas. For these categories, the weather conditions are compared with those at the primary checkpoint. (**g**) Soil moisture *regional* estimation (*Re*) for simulated areas.

In Figure 9a, changes in the landscape features are simulated: image I presents an area with the original landscape; image II shows the modified original landscape so that the grassland prevails; and, in image III, after the modifications, the tree-covered areas prevail. Moreover, Figure 9b–f present the temperature (C^r_1), rain (C^r_2), solar radiation (C^r_3), wind speed (C^r_4), and evapotranspiration (C^r_5) for each category: the original landscape, grassland, and tree-covered areas. For these categories, the weather conditions are compared with the weather conditions at the primary checkpoint P^0. Finally, Figure 9g presents the soil moisture *regional* estimation (Re) for the simulated areas.

The simulation highlights how changes in the landscape features impact the weather conditions and soil moisture. Section 2.2.1 **D** and Section 3.2.1 **B** presented the landscape adjustment and weather conditions adjustment, respectively, explaining that there are two adjustment factors for the weather conditions. The first is derived from steady adjustment, which analyzes the landscape features of the estimation region and its influence over the weather conditions. The second is obtained from variable adjustment, which considers the interactions among the weather conditions. Using a fuzzy inference system, the adjustment factor is the result of the comparison of the characteristics of the sector under analysis and the primary checkpoint P^0 (where the weather conditions are measured). Therefore, the linguistic variables refer to the values of the weather conditions (C^r_i) analyzed in the sector $s(x, y)$ and whether they are lower, equal to or higher than the values of the weather conditions at the primary checkpoint P^0.

For example, in Figure 9b, for the temperature (C^r_1), column II (mainly grassland) has more sectors with equal adjustments than the original landscape (column I). On the other hand, column III (tree-covered areas) has more sectors with lower adjustments than the original landscape (column I).

Similarly, in Figure 9d, for solar radiation (C^r_3), column II (mainly grassland) has more sectors with equal adjustments than the original landscape (column I); likewise, there are sectors with higher adjustments. Column III (tree-covered areas) has more sectors with lower adjustments than the original landscape (column I). Reasonable results can be observed in Figure 9c,e,f. For example, in Figure 9f, column II has more sectors with evapotranspiration (C^r_5) with equal and higher adjustments than the original landscape (column I), since this area is mainly grassland. We note again that all lower, equal or higher adjustments are with respect to the primary checkpoint P^0 (where the weather conditions are measured).

Finally, Figure 9g compares the soil moisture *regional* estimation (Re) concerning the primary checkpoint P^0. Column III (tree-covered areas) has more sectors with higher humidity.

The results of soil moisture were compared indirectly with interpolation methods; however, these interpolation methods show limitations when used in a regional estimation as proposed in this study because spatial interpolation models use a network of measurement points; rainfall is not remarkably homogenous in a region, thus basing its interpolation value only on spatial measurements or statistical records can be misleading.

This new *regional* soil moisture estimation method uses an intelligent adjustment of weather conditions based on spatial features. The *regional* estimation of soil moisture depends on the accuracy of the intelligent adjustment of weather conditions based on spatial features [39] and the fuzzy *point* estimation based on decision-making, validated in [32]. In [39], Tables 10–14 compared weather conditions adjusted, measured, and interpolated for temperature, rain, solar radiation, wind speed, and evapotranspiration, respectively. All cases highlight the advantage of using an intelligent adjustment of weather conditions based on spatial features; therefore, the regional estimation of soil moisture will depend on the accuracy of those results and will be best.

5. Conclusions

A new method, named the integrated approach, to obtain a *regional* soil moisture estimation is developed in this study. This method has been tested over several years by comparing the results of soil moisture *regional* estimation with measurements at many points in the study region. The integrated approach achieves a *regional* soil moisture estimation as a set of soil moisture *point* estimates. The method can detect when the soil moisture is deficient in a region, allowing actions to prevent water stress. A regional estimate can reduce an irrigation system's operational and maintenance complexity.

This new method exploits the advantages of FEADM, such as obtaining a quantitative estimate of the soil moisture and avoiding the complexity involved in measuring it. Likewise, by combining IWeCASF and FEADM, this integrated approach addresses the input acquisition for FEADM; consequently, FEADM can obtain soil moisture *point* estimates at several checkpoints scattered within an estimation region.

FEADM and IWeCASF are two computer methods already presented in the literature, but they had not been integrated as part of a single method, as proposed in this work.

Furthermore, the integrated approach allows the more accessible display of the relationships among the weather conditions, landscape features and soil moisture content. Some weather conditions, such as rain $C^r_{i=2}$, exert a greater influence over the soil moisture content; for example, when there is rainfall, the soil moisture content is high. In addition, the landscape features, such as tree-covered areas $(F^{t=2})$, can also modify the soil moisture content because solar radiation does not fully reach the soil.

This new method based on linking FEADM with IWeCASF allowed *regional* soil moisture estimation, reducing the implementation and maintenance complexity of conventional automatic irrigation systems and their inherent costs. Although the experimental case study was for a specific region, this integrated approach can be applied in any estimation region with the required input data (satellite imagery, crop and soil data, weather conditions measured at a single checkpoint, and irrigation water record).

IWeCASF justifies the advantage of using an intelligent adjustment of weather conditions based on spatial features. Therefore, linking FEADM-IWeCASF for the *regional* soil moisture estimation will be better than interpolation methods. All of the above verify compliance with the hypotheses proposed for this work.

However, as a limitation, we point out that the experimental case study was for the region of Figure 1. Other experimental case studies in different regions are already being performed, and the analysis of their results is considered future work.

Author Contributions: Conceptualization, methodology, investigation, supervision, validation, funding acquisition, project administration, and review and editing, L.P.S.-F. Conceptualization, investigation, methodology, data acquisition, formal analysis, validation, software, visualization,

and writing—original draft preparation, D.A.F.-C. Conceptualization, methodology, investigation, supervision, validation, and review and editing, L.A.S.-P. All authors have read and agreed to the published version of the manuscript.

Funding: This research was funded by the Instituto Politécnico Nacional of Mexico and the National Council of Humanities, Science and Technology (CONAHCYT) of Mexico. SIP 20241747 and SIP 20231285.

Data Availability Statement: The software used is MATLAB 2022, and it is available under license. The same applies to QML (Qt Modeling Language) and Limbo. Online data and codes are available: https://github.com/Lsanchez2024/An-integrated-approach-for-regional-estimations-of-soil-moisture- (accessed on 18 September 2024).

Acknowledgments: We thank the Instituto Politécnico Nacional, Mexico and the National Council of Humanities, Science and Technology (CONAHCYT) of Mexico for their financial support.

Conflicts of Interest: The authors declare no conflicts of interest.

Appendix A. Color Space Image Conversion

A color space conversion, as shown in Figure A1, highlights the landscape features of an estimation region. The colors that represent each landscape feature F^l are more distinguishable. As a result, better color segmentation is performed.

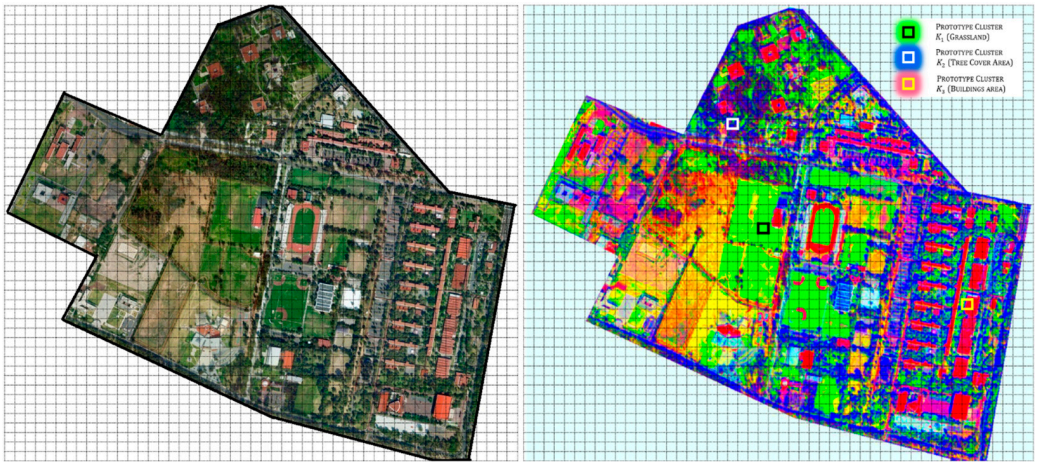

(**a**) (**b**)

Figure A1. Estimation region. (**a**) The original image is in RGB color space. (**b**) Image in CIELAB color space under decorrelation used to obtain landscape matrices $F^{l=1,2,3}$.

References

1. Goumopoulos, C.; O'Flynn, B.; Kameas, A. Automated zone-specific irrigation with wireless sensor/actuator network and adaptable decision support. *Comput. Electron. Agric.* **2014**, *105*, 20–33. [CrossRef]
2. Adeyemi, O.; Grove, I.; Peets, S.; Norton, T. Advanced Monitoring and Management Systems for Improving Sustainability in Precision Irrigation. *Sustainability* **2017**, *9*, 353. [CrossRef]
3. Lloret, J.; Sendra, S.; Garcia, L.; Jimenez, J.M. A Wireless Sensor Network Deployment for Soil Moisture Monitoring in Precision Agriculture. *Sensors* **2021**, *21*, 7243. [CrossRef]
4. El Mezouari, A.; El Fazziki, A.; Sadgal, M. Smart Irrigation System. *IFAC-PapersOnLine* **2022**, *55*, 3298–3303. [CrossRef]
5. Phasinam, K.; Kassanuk, T.; Shinde, P.P.; Thakar, C.M.; Sharma, D.K.; Mohiddin, M.K.; Rahmani, A.W. Application of IoT and Cloud Computing in Automation of Agriculture Irrigation. *J. Food Qual.* **2022**, *2022*, 8285969. [CrossRef]
6. Sánchez-Sutil, F.; Cano-Ortega, A. Smart Control and Energy Efficiency in Irrigation Systems Using LoRaWAN. *Sensors* **2021**, *21*, 7041. [CrossRef] [PubMed]
7. Abioye, E.A.; Abidin, M.S.Z.; Mahmud, M.S.A.; Buyamin, S.; Ishak, M.H.I.; Rahman, M.K.I.A.; Otuoze, A.O.; Onotu, P.; Ramli, M.S.A. A review on monitoring and advanced control strategies for precision irrigation. *Comput. Electron. Agric.* **2020**, *173*, 105441. [CrossRef]
8. Raouhi, E.M.; Zouizza, M.; Lachgar, M.; Zouani, Y.; Hrimech, H.; Kartit, A. AIDSII: An AI-based digital system for intelligent irrigation. *Softw. Impacts* **2023**, *17*, 100574. [CrossRef]
9. Moradkhani, H. Hydrologic remote sensing and land surface data assimilation. *Sensors* **2008**, *8*, 2986–3004. [CrossRef]

10. Crow, W.T.; Chen, F.; Reichle, R.H.; Liu, Q. L band microwave remote sensing and land data assimilation improve the representation of prestorm soil moisture conditions for hydrologic forecasting. *Geophys. Res. Lett.* **2017**, *44*, 5495–5503. [CrossRef]
11. Phillips, A.J.; Newlands, N.K.; Liang, S.H.L.; Ellert, B.H. Integrated sensing of soil moisture at the field-scale: Measuring, modeling and sharing for improved agricultural decision support. *Comput. Electron. Agric.* **2014**, *107*, 73–88. [CrossRef]
12. Romero, R.; Muriel, J.L.; García, I.; Muñoz de la Peña, D. Research on automatic irrigation control: State of the art and recent results. *Agric. Water Manag.* **2012**, *114*, 59–66. [CrossRef]
13. Millán, S.; Casadesús, J.; Campillo, C.; Moñino, M.J.; Prieto, M.H. Using Soil Moisture Sensors for Automated Irrigation Scheduling in a Plum Crop. *Water* **2019**, *11*, 2061. [CrossRef]
14. Aubert, D.; Loumagne, C.; Oudin, L. Sequential assimilation of soil moisture and streamflow data in a conceptual rainfall–runoff model. *J. Hydrol.* **2003**, *280*, 145–161. [CrossRef]
15. Perrin, C.; Michel, C.; Andréassian, V. Does a large number of parameters enhance model performance? Comparative assessment of common catchment model structures on 429 catchments. *J. Hydrol.* **2001**, *242*, 275–301. [CrossRef]
16. Agyeman, B.T.; Bo, S.; Sahoo, S.R.; Yin, X.; Liu, J.; Shah, S.L. Soil moisture map construction by sequential data assimilation using an extended Kalman filter. *J. Hydrol.* **2021**, *598*, 126425. [CrossRef]
17. Jones, H.G. Irrigation scheduling: Advantages and pitfalls of plant-based methods. *J. Exp. Bot.* **2004**, *55*, 2427–2436. [CrossRef]
18. Pan, F.; Nieswiadomy, M.; Qian, S. Application of a soil moisture diagnostic equation for estimating root-zone soil moisture in arid and semi-arid regions. *J. Hydrol.* **2015**, *524*, 296–310. [CrossRef]
19. Gu, Z.; Qi, Z.; Burghate, R.; Yuan, S.; Jiao, X.; Xu, J. Irrigation Scheduling Approaches and Applications: A Review. *J. Irrig. Drain. Eng.* **2020**, *146*, 04020007. [CrossRef]
20. Kumar, S.V.; Dirmeyer, P.A.; Peters-Lidard, C.D.; Bindlish, R.; Bolten, J. Information theoretic evaluation of satellite soil moisture retrievals. *Remote Sens. Environ.* **2018**, *204*, 392–400. [CrossRef]
21. Beck, H.E.; Pan, M.; Miralles, D.G.; Reichle, R.H.; Dorigo, W.A.; Hahn, S.; Sheffield, J.; Karthikeyan, L.; Balsamo, G.; Parinussa, R.M.; et al. Evaluation of 18 satellite- And model-based soil moisture products using in situ measurements from 826 sensors. *Hydrol. Earth Syst. Sci.* **2021**, *25*, 17–40. [CrossRef]
22. Jarray, N.; Ben Abbes, A.; Rhif, M.; Dhaou, H.; Ouessar, M.; Farah, I.R. SMETool: A web-based tool for soil moisture estimation based on Eo-Learn framework and Machine Learning methods. *Environ. Model. Softw.* **2022**, *157*, 105505. [CrossRef]
23. Pulvirenti, L.; Squicciarino, G.; Cenci, L.; Boni, G.; Pierdicca, N.; Chini, M.; Versace, C.; Campanella, P. A surface soil moisture mapping service at national (Italian) scale based on Sentinel-1 data. *Environ. Model. Softw.* **2018**, *102*, 13–28. [CrossRef]
24. Tischler, M.; Garcia, M.; Peters-Lidard, C.; Moran, M.S.; Miller, S.; Thoma, D.; Kumar, S.; Geiger, J. A GIS framework for surface-layer soil moisture estimation combining satellite radar measurements and land surface modeling with soil physical property estimation. *Environ. Model. Softw.* **2007**, *22*, 891–898. [CrossRef]
25. Souissi, R.; Al Bitar, A.; Zribi, M. Accuracy and Transferability of Artificial Neural Networks in Predicting in Situ Root-Zone Soil Moisture for Various Regions across the Globe. *Water* **2020**, *12*, 3109. [CrossRef]
26. Ghasemloo, N.; Matkan, A.A.; Alimohammadi, A.; Aghighi, H.; Mirbagheri, B. Estimating the Agricultural Farm Soil Moisture Using Spectral Indices of Landsat 8, and Sentinel-1, and Artificial Neural Networks. *J. Geovisualiz. Spat. Anal.* **2022**, *6*, 1–12. [CrossRef]
27. Han, H.; Choi, C.; Kim, J.; Morrison, R.R.; Jung, J.; Kim, H.S.; Han, H.; Choi, C.; Kim, J.; Morrison, R.R.; et al. Multiple-Depth Soil Moisture Estimates Using Artificial Neural Network and Long Short-Term Memory Models. *Water* **2021**, *13*, 2584. [CrossRef]
28. Yu, Z.; Liu, D.; Lü, H.; Fu, X.; Xiang, L.; Zhu, Y. A multi-layer soil moisture data assimilation using support vector machines and ensemble particle filter. *J. Hydrol.* **2012**, *475*, 53–64. [CrossRef]
29. He, B.; Jia, B.; Zhao, Y.; Wang, X.; Wei, M.; Dietzel, R. Estimate soil moisture of maize by combining support vector machine and chaotic whale optimization algorithm. *Agric. Water Manag.* **2022**, *267*, 107618. [CrossRef]
30. Liu, D.; Mishra, A.K.; Yu, Z. Evaluating uncertainties in multi-layer soil moisture estimation with support vector machines and ensemble Kalman filtering. *J. Hydrol.* **2016**, *538*, 243–255. [CrossRef]
31. Zhu, Q.; Wang, Y.; Luo, Y. Improvement of multi-layer soil moisture prediction using support vector machines and ensemble Kalman filter coupled with remote sensing soil moisture datasets over an agriculture dominant basin in China. *Hydrol. Process.* **2021**, *35*, e14154. [CrossRef]
32. Flores-Carrillo, D.A.; Sánchez-Fernández, L.P.; Sánchez-Pérez, L.A.; Carbajal-Hernández, J.J. Soil moisture Fuzzy Estimation Approach based on Decision-Making. *Environ. Model. Softw.* **2017**, *91*, 223–240. [CrossRef]
33. Wang, S.; Li, R.; Wu, Y.; Wang, W. Estimation of surface soil moisture by combining a structural equation model and an artificial neural network (SEM-ANN). *Sci. Total Environ.* **2023**, *876*, 162558. [CrossRef] [PubMed]
34. Kambalimath, S.; Deka, P.C. A basic review of fuzzy logic applications in hydrology and water resources. *Appl. Water Sci.* **2020**, *10*, 1–14. [CrossRef]
35. Rodríguez-Pérez, A.M.; Rodríguez-Gonzalez, C.A.; López, R.; Hernández-Torres, J.A.; Caparrós-Mancera, J.J. Water Microturbines for Sustainable Applications: Optimization Analysis and Experimental Validation. *Water Resour. Manag.* **2024**, *38*, 1011–1025. [CrossRef]
36. Rodríguez-Pérez, Á.M.; García-Chica, A.; Caparros-Mancera, J.J.; Rodríguez, C.A. Turbine-Based Generation in Greenhouse Irrigation Systems. *Hydrology* **2024**, *11*, 149. [CrossRef]

37. Elshorbagy, A.; Parasuraman, K. On the relevance of using artificial neural networks for estimating soil moisture content. *J. Hydrol.* **2008**, *362*, 1–18. [CrossRef]
38. Ondieki, J.; Laneve, G.; Marsella, M.; Mito, C.; Ondieki, J.; Laneve, G.; Marsella, M.; Mito, C. Enhancing Surface Soil Moisture Estimation through Integration of Artificial Neural Networks Machine Learning and Fusion of Meteorological, Sentinel-1A and Sentinel-2A Satellite Data. *Adv. Remote Sens.* **2023**, *12*, 99–122. [CrossRef]
39. Sánchez-Fernández, L.P.; Flores-Carrillo, D.A.; Sánchez-Pérez, L.A. Computer Model for an Intelligent Adjustment of Weather Conditions Based on Spatial Features for Soil Moisture Estimation. *Mathematics* **2024**, *12*, 152. [CrossRef]
40. Welcome to the QGIS Project! Available online: https://qgis.org/en/site/ (accessed on 22 December 2023).
41. Sridhar, V.; Hubbard, K.G.; You, J.; Hunt, E.D. Development of the Soil Moisture Index to Quantify Agricultural Drought and Its "User Friendliness" in Severity-Area-Duration Assessment. *J. Hydrometeorol.* **2008**, *9*, 660–676. [CrossRef]
42. Saha, A.; Patil, M.; Goyal, V.C.; Rathore, D.S. Assessment and Impact of Soil Moisture Index in Agricultural Drought Estimation Using Remote Sensing and GIS Techniques. *Proceedings* **2018**, *7*, 2. [CrossRef]
43. WCA 2020 | World Programme for the Census of Agriculture | Food and Agriculture Organization of the United Nations. Available online: https://www.fao.org/world-census-agriculture/wcarounds/wca2020/en/ (accessed on 28 November 2023).
44. CIE Publications—Premium Source for Knowledge on Light and Lighting | CIE. Available online: https://cie.co.at/publications (accessed on 11 December 2023).
45. Chang, D.-Y. Applications of the extent analysis method on fuzzy AHP. *Eur. J. Oper. Res.* **1996**, *95*, 649–655. [CrossRef]
46. Şen, C.G.; Çınar, G. Evaluation and pre-allocation of operators with multiple skills: A combined fuzzy AHP and max–min approach. *Expert Syst. Appl.* **2010**, *37*, 2043–2053. [CrossRef]
47. Wang, Y.M.; Luo, Y.; Hua, Z. On the extent analysis method for fuzzy AHP and its applications. *Eur. J. Oper. Res.* **2008**, *186*, 735–747. [CrossRef]
48. Liou, T.-S.; Wang, M.-J.J. Ranking fuzzy numbers with integral value. *Fuzzy Sets Syst.* **1992**, *50*, 247–255. [CrossRef]